Aalto University
School of Chemical
Engineering

Mingyu Han

SYNTHESIS AND CHARACTERIZATION OF CELLULOSE-DERIVED POLYMERS FOR THE TREATMENT OF DAMAGED CARTILAGE

Nordic Master Programme in Polymer Technology

Major in Biomaterials Science

Master's thesis for the degree of Master of Science in Technology submitted for inspection, Espoo, 15 May 2017.

Supervisor Professor Monika Österberg

Instructor PhD. Juan José Valle-Delgado

Aalto University
School of Chemical
Engineering

Aalto University, P.O. BOX 11000, 00076 AALTO
www.aalto.fi

Abstract of master's thesis

Author Mingyu Han

Title of thesis Synthesis and characterization of cellulose-derived polymers for the treatment of damaged cartilage

Degree Programme Nordic Master Program in Polymer Technology

Major Biomaterials Science

Thesis supervisor Professor Monika Österberg

Thesis advisor(s) / Thesis examiner(s) PhD. Juan José Valle-Delgado

Date 15.05.2017 **Number of pages** 61 **Language** English

Abstract

Carboxymethyl cellulose (CMC) is currently the most widely used cellulose derivative and considered as a promising biomaterial due to its biocompatibility, biodegradability and non-toxicity. Polyethylene glycol grafted carboxymethyl cellulose (CMC-g-PEG) has been proved to be a very lubricating polymer.

This MSc. thesis work aims to study further the potential application of the lubricating CMC-g-PEG for the treatment of damaged cartilage. CMC-g-PEG with different PEG chain lengths were successfully synthesized and characterized by conductometric titration and Fourier transform infrared spectroscopy. Polyethylene glycol grafted dialdehyde carboxymethyl cellulose (DCMC-g-PEG) was synthesized by oxidation of CMC-g-PEG with sodium periodate.

The adsorption of the different polymers on collagen IV films (first approach model for cartilage) was studied by quartz crystal microbalance with dissipation. Compared with dialyzed CMC and CMC-g-PEG, much more DCMC-g-PEG absorbed onto the surface of collagen IV films due to the existence of covalently binding between aldehyde groups of DCMC-g-PEG and amine groups of collagens. The adsorption results of CMC-g-PEG and DCMC-g-PEG provide the evidence that the introduction of aldehyde groups to the backbone of CMC-g-PEG can improve its attaching ability to collagen IV.

Keywords CMC, CMC-g-PEG, DCMC-g-PEG, osteoarthritis, cartilage, attaching ability

Acknowledgments

This master thesis has been conducted in the Department of Bioproducts and Biosystems at Aalto University, School of Chemical Engineering between November 2016 and May 2017. The master thesis work is part of a collaboration between Aalto University and the University of Helsinki.

Firstly, I want to thank my advisor, Juan José Valle-Delgado, for giving me lots of support and useful suggestions when I needed it during the literature review and experimental part of the thesis. Further, I really appreciate my supervisor, Monika Österberg, for the opportunity to accomplish my master thesis work in her research group and for all her support.

Secondly, I want to thank all the research staffs for teaching me how to operate the equipment and sharing their valuable experiences with me.

Furthermore, thanks both Aalto University and Chalmers University of Technology for offering this great master program. I learn not only knowledge from this two world-leading universities, but also interesting culture from Finland and Sweden.

Last but not least, I want to thank my parents and my girlfriend, Hui, for supporting and encouraging me when I was in bad mood during the master thesis work. I love you!

Mingyu Han

15.05.2017

Contents

Abbreviations

1-ethyl-3-(3-dimethylaminopropyl) carbodiimide hydrochloride	EDC
Alginate dialdehyde	ADA
Body mass index	BMI
Carboxymethyl cellulose	CMC
Cellulose nanofibrils	CNF
Dialdehyde carboxymethyl cellulose	DCMC
Disease-modifying osteoarthritis drugs	DMOADs
European League Against Rheumatism	EULAR
Extracellular matrix	ECM
Fourier transform infrared	FTIR
Glacial acetic acid	CH_3COOH
Hyaluronic acid	HA
Hydrochloric acid	HCl
Methoxy polyethylene glycol amine	OMe-PEG-amine
Monopotassium phosphate	KH_2PO_4
Monosodium phosphate	NaH_2PO_4
Nanoembossed polycaprolactone	NPCL
Nanoembossed polyurethane	NPU
N-hydroxysuccinimide	NHS
Non-steroidal anti-inflammatory agents	NSAIDs
Osteoarthritis Research Society International	OARSI
Osteoarthritis	OA

Phosphate buffered saline	PBS
Poly(2-methyloxazoline)	PMOXA
Poly(glutamic acid)	PGA
Poly(lactic acid)	PLA
Poly(lactic acid-co-glycolic acid)	PLGA
Poly(L-lysine)-graft-poly(ethylene glycol)	PLL-g-PEG
Polyacrylic acid	PAA
Polyethylene glycol grafted carboxymethyl cellulose	CMC-g-PEG
Polyethylene glycol grafted dialdehyde carboxymethyl cellulose	DCMC-g-PEG
Polyethylene glycol	PEG
Polyvinyl alcohol	PVA
Polyvinylpyrrolidone	PVP
Potassium bromide	KBr
Quartz Crystal Microbalance with Dissipation monitoring	QCM-D
Quartz Crystal Microbalance	QCM
Sodium acetate trihydrate	$CH_3COONa*3H_2O$
Sodium chloride	NaCl
Sodium hydroxide	NaOH
Sodium periodate	$NaIO_4$
Superficial zone protein	SZP
Symptomatic slow-acting drugs for osteoarthritis	SYSADOA

1. Introduction

There are different kinds of diseases such as costochondritis, achondroplasia and osteoarthritis which may cause cartilage damage. Costochondritis describes inflammation of the cartilage in the ribs. Pain is produced when the affected cartilage segments are palpated and it may radiate on the chest wall. So far there is no clinical treatment for this kind of disease. The normal treatments are reducing the frequency or intensity of exercise or work activities and applying heat with compresses to help the overused muscle particularly. (Proulx and Zryd 2009). As the most common genetic form of dwarfism, achondroplasia is a condition where the chondrocytes within the cartilage fail to proliferate and the epiphyseal plate of long bones near the joints are particularly affected. These plates are important in bone growth and development and the condition can cause dwarfism (Horton *et al*. 2007). However, among these cartilage-related diseases, osteoarthritis (OA) is the most common form of disabling joint disease (Buckwalter and Mankin 1998). It is accepted that OA is a type of disease related to articular cartilage. About 10-12% of the adult people has symptomatic OA, and the number of people who is suffering OA will be doubled by the year 2020 because of the sharply increasing prevalence of obesity and the 'baby boomer' generation. For the people aged 65 or over, the risk of mobility disability attributable to OA is much higher than due to any other kind of medical conditions. The increasing number of people who is suffering OA will seriously impact the fragile health-care system which is spending 1-2% of the gross domestic product in most western countries (Hunter 2011).

Since there is not a specific medicine that could cure OA, it is essential to develop a new kind of system for the treatment of damaged cartilage. Our approach is based on the use of carboxymethyl cellulose (CMC), which is considered as a promising natural polymer that can be used in biomedical applications. In this project, we have synthesized a type of brush-like polymer by using carboxymethyl cellulose as the backbone and polyethylene glycol (CMC-g-PEG) as the side chain, which may be used as a potential treatment for damaged cartilages due to its remarkable lubrication properties. Two types of CMC-g-PEG were synthesized with different PEG lengths. CMC-g-PEG was then transformed into dialdehyde CMC-g-PEG (DCMC-g-PEG) by reacting with sodium periodate to improve the attachment of the polymers to cartilage tissues. Finally, the adsorption of the synthesized CMC-g-PEG and DCMC-g-PEG on

collagen films (first approach model for cartilage) was studied by using quartz crystal microbalance with dissipation monitoring, which is a relatively new type of technology in the study of the biomedical area, especially in the adsorption of polymers to the bioactive tissue.

2. Literature review

2.1 Cartilage and osteoarthritis

2.1.1 Cartilage: composition, structure and properties.

There are three types of cartilages in the human body. The cartilage found in articulating joints, nose, trachea, intervertebral disks and vertebral endplates is called hyaline cartilage. Another kind of cartilage found in the tendon, ligament insertion site and the meniscus is called elastic cartilage which contains elastic fibres besides collagen and proteoglycan. The other type of cartilage is named fibrocartilage, which is found only in ears (Spiller *et al.* 2011). Articular cartilage is a 2 to 4 mm thick tissue that covers and protects the bones in the joints (Figure 1). The composition of articular cartilage includes an extracellular matrix (ECM) which contains water, collagen, proteoglycans, and other small amounts of noncollagenous proteins and glycoproteins. Also, there is a rare distribution of cells named chondrocytes which are highly specialized (Fox *et al*. 2009). The composition and structure of ECM of articular cartilage are associated with its biomechanical function including lubrication, wear resistance, bear loading and shock absorption (Doulabi *et al*. 2014).

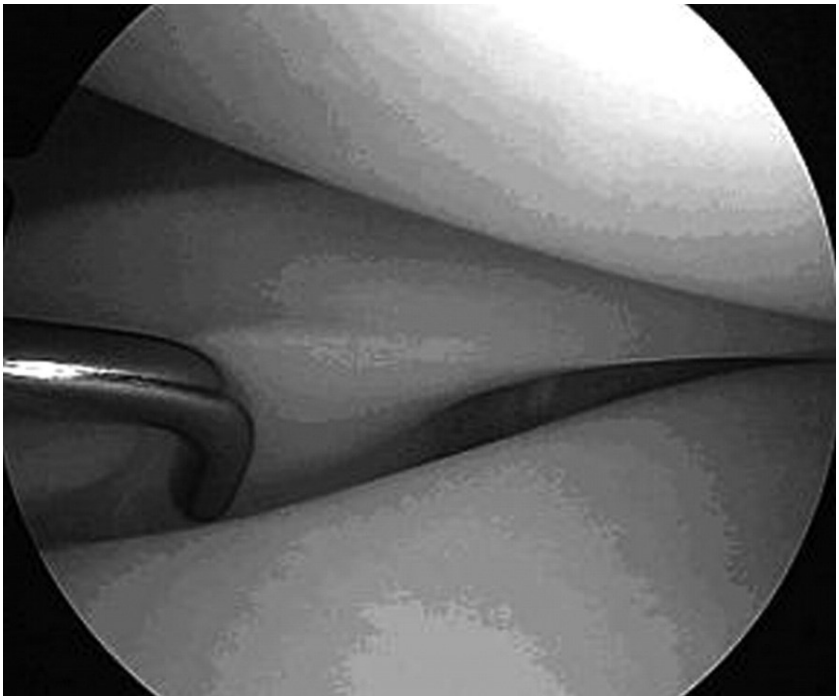

Figure 1. Healthy articular cartilage in an adult knee (Fox *et al*. 2009).

Articular cartilage contains a relatively small percentage of chondrocytes, which are originated from stem cells. These cells are surrounded by a multicomponent matrix. The proteoglycan represents almost 30% of the dry weight of articular cartilage. However, the proteoglycan concentration and water content are different at different depths of the articular cartilage. The content of proteoglycan increases from the articular surface to the deeper regions of the cartilage. Proteoglycans have a bottlebrush-like structure which contains a protein core with attached chains of chondroitin sulfate and keratan sulfate. These bottlebrush-like proteoglycans bind to the hyaluronic acid backbone to form a macromolecule (Figure 2) (Mansour 2003). Hyaluronic acid is a macromolecular polysaccharide of repeating disaccharide units of N-acetyl-d- glucosamine and d-glucuronic acid and it is present in connective tissues like cartilage (Bauer *et al*. 2016). Collagen is a fibrous protein, which is also the most abundant structural macromolecule in the animal kingdom. It makes up to 60 to 70% of the dry weight of the whole tissue, but the architecture varies through the depth of the articular cartilage. Type II collagen represents 90 to 95% of the collagen, although collagen types I, IV, V, VI, IX, and XI are also present in relatively small proportion (Fox *et al.* 2009). Water represent approximately 70 to 85% of the weight of the

whole articular cartilage (Mansour 2003). Approximately 70% of water is stored in the pore space of the matrix, and the remainder is contained in intrafibrillar and intracellular space. The transportation of nutrients to chondrocytes and lubrication is achieved by the flow of water through cartilage. Water in the articular cartilage also plays a significant role to withstand large load through the combination of pressurization within the matrix and frictional resistance to water flow (Fox *et al*. 2009).

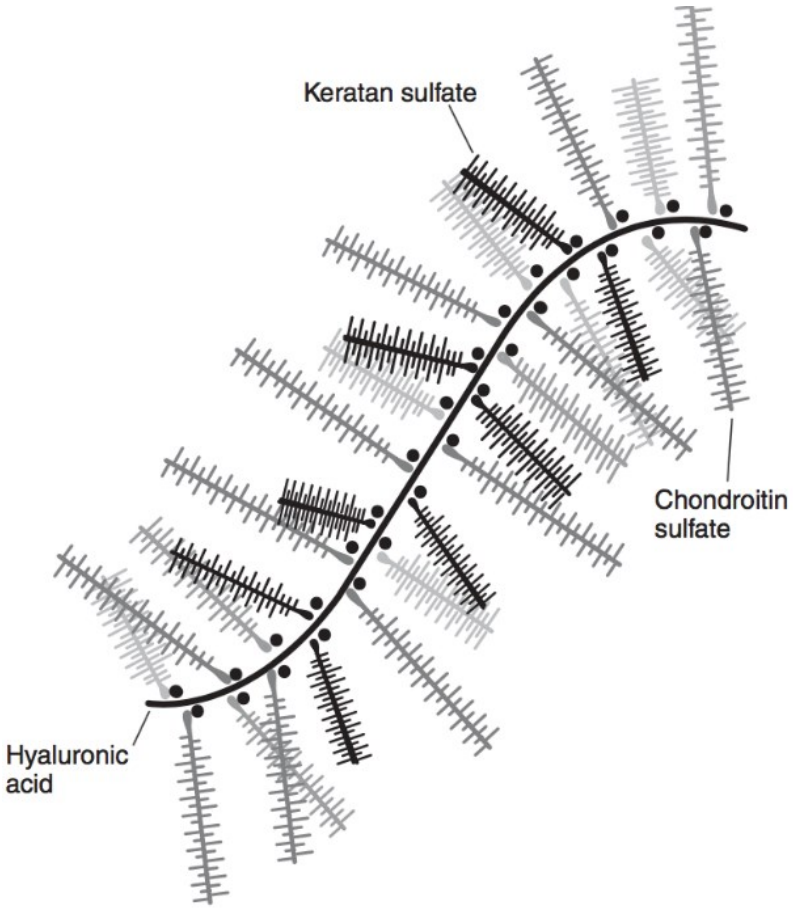

Figure 2. The bottlebrush-like structure of proteoglycans and how they bind to hyaluronic acid (Mansour 2003).

The articular cartilage is divided into three zones which are the superficial zone, the middle zone, and the deep zone (Figure 3). The superficial zone represents almost 10% to 20% of the articular cartilage thickness, and it contains a large number of chondrocytes. Due to the existence of dense thin collagen fibrils parallel to the articular surface, the superficial zone is

responsible for the tensile properties to enable the articular cartilage to resist the shear, tensile and compressive forces. It also protects and maintains the deeper layers of the articular cartilage (Fox *et al*. 2009). The middle zone represents 40%-60% of the total thickness. In the middle zone, cells have a spheroidal shape and appear randomly distributed in less parallel thick collagen fibrils. The proteoglycan content is the highest and the cell density is much lower than in the superficial zone (Doulabi *et al*. 2014). The middle zone is the first line to resist compressional forces functionally and acts as an anatomic bridge between the superficial zone and the deep zone (Fox *et al*. 2009). The deep zone (about 30% volume of the cartilage) contains thick collagen fibrils perpendicular to the articular surface, the lowest water content, the lowest cell density compared with other zones and much lower content of proteoglycan than in the middle zone (Doulabi *et al*. 2014). The main role of the deep zone is to resist compression forces (Fox *et al*. 2009). The tidemark separates the deep zone and the calcified cartilage, which is the boundary between the cartilage and the subchondral bone and is responsible for anchoring the cartilage to the bone (Mansour 2003).

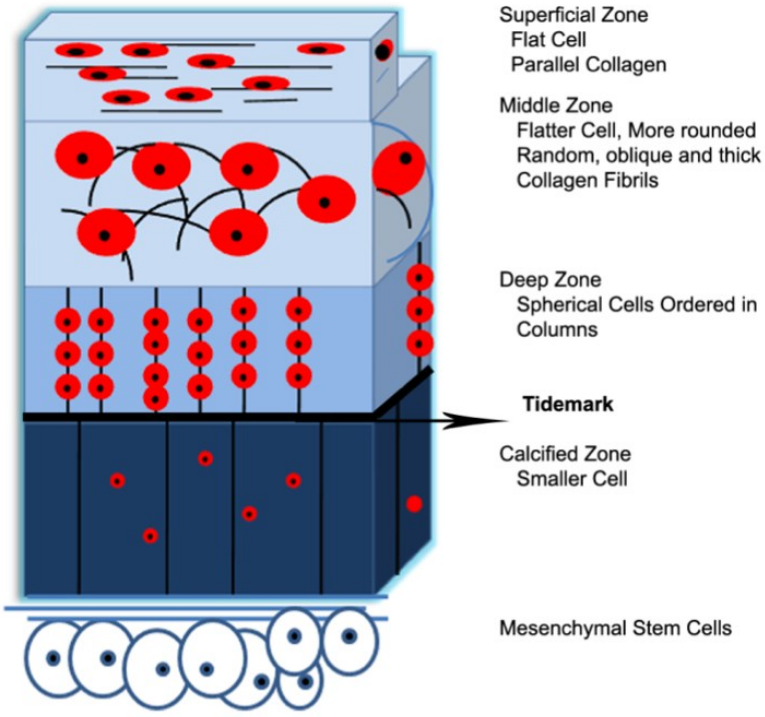

Figure 3. Zone distribution in a healthy articular cartilage (Doulabi *et al*. 2014).

It is widely accepted that articular cartilage exhibits a range of complex characteristics and behaviors (Ateshian 2009). The most significant function of articular cartilage is to protect the subchondral bone from damage caused by connecting with other bones directly. During physical activities, large forces are encountered by the joints, especially the load bearing joints like knee and hip (Eckstein *et al*. 1999). Articular cartilage provides a smooth, lubricated surface, and it is responsible for the transmission of loads to the underlying subchondral bone (Fox *et al*. 2009). Since different depth of the articular cartilage shows different composition and organization (Doulabi *et al*. 2014), there is a quantitative association between the properties of articular cartilage and the content of glycosaminoglycan, collagen and water (Mansour 2003).

The cartilage provides the joint with essential biomechanical functions, such as wear resistance, load bearing, and shock absorption (Lu, Mow 2008). Cartilage is a viscoelastic and porous material filled with fluid. When the compression is applied, the articular cartilage will firstly support the load by building the interstitial hydrostatic fluid pressure in the tissue, the interstitial fluid is then redistributed within the matrix and the cartilage begins to deform. Finally, fluid flow stops since the hydrostatic pressure decreases to zero, and the entire load is carried by the solid cartilage matrix (Eckstein *et al*. 1999). However, the compressive stiffness of cartilage increases as a function of the total glycosaminoglycan content. (Mansour 2003). Also, articular cartilage shows a creep and stress-relaxation response. The deformation of cartilage keeps increasing with time when a constant compressive stress is applied to the tissue, and the cartilage will creep until an equilibrium value is reached. Similarly, when cartilage is carried a constant strain, the stress will rise to a peak and then a slow stress-relaxation process will happen before an equilibrium value is reached (Fox *et al*. 2009).

Articular cartilage is also a lubricious tissue which can provide low-friction to the joint by combining two lubrication mechanisms named fluid film-lubricated model and boundary lubrication model (Schmidt *et al*. 2007). The fluid film-lubricated model relies on the fluid forces and rheological phenomena, and it includes hydrostatic and hydrodynamic mechanisms. Hydrostatic mechanism indicates that the opposing surfaces are separated by an externally pressurized fluid film, and fluid film forces are generated by the sliding speed of articulating surfaces in the hydrodynamic mechanism. However, several studies show that the boundary lubrication plays more important role in cartilage tissue (Jahn *et al*. 2016),

especially in the condition of low sliding speed, high load and low fluid viscosity. The boundary lubrication between the articulating surfaces is controlled by a sacrificial layer of adsorbed boundary lubricant: hyaluronic acid, surface active phospholipids and lubricin (McNary *et al*. 2012). The lubricating properties of hyaluronic acid have been well documented in the literature (Benz *et al*. 2004, Greene *et al*. 2014, Seror *et al*. 2011, Valle-Delgado *et al*. 2016). However, some studies also point that hyaluronic acid is not a sole cartilage lubricant, which means that there is an interaction between hyaluronic acid and other components like lubricin and surface-active phospholipids when it acts as boundary lubricant (Yu *et al*. 2012). Surface-active phospholipids are present in synovial fluid of normal joint in considerable quantities (Hills and Crawford 2003), and they include two types which are called phosphatidylcholines and non-phosphatidylcholines (Gale *et al*. 2007). Surface-active phospholipids are responsible for making tissues more hydrophobic by their adsorption on the tissue surface (Hills, B. A. 2002). Therefore, there are various investigations undertaken to explore the possibilities to use surface-active phospholipid as a method to improve the tribological sliding behavior of cartilage (Ozturk *et al*. 2004). Lubricin is a cytoprotective glycoprotein that is responsible for the significant boundary lubrication mechanisms. Therefore, the loss of lubricin function is considered as a contributing factor for the development of joint diseases like OA. Lubricin is also described as superficial zone protein (SZP) since it is synthesized and localized in the superficial layer of articular cartilage and occurs as a soluble component of synovial fluid. Based on an abundant number of studies including human genetic disorder, rodent gene knockout models, animal models of arthritis and functional tribological study, it is widely accepted that lubricin is a critical lubricant for articular cartilage (McNary *et al*. 2012, Lee *et al.* 2008 and Jones *et al.* 2007). Lubricin can act as an efficient boundary lubricant, and facilitate the generation of negative electrostatic repulsion forces between opposing cartilage surfaces (Jones *et al*. 2007).

2.1.2 Osteoarthritis (OA)

OA is considered as a kind of heterogeneous disease which is characterised by the failure of the synovial joint organ. For instance, when the joint tissues cannot tolerate the applied mechanical stress, the severe OA of the knee develops since the cartilage has a very limited capacity for self-repair. For every 1 kg of weight carried by the body, the contact load across

the knee joint experiences four times that load. By comparing the healthy knee joint with the osteoarthritic knee (Figure 4), OA is characterised by cartilage loss, bone remodelling and sclerosis, meniscal damage, synovial hypertrophy, osteophytes and ligament dysfunction (Hunter 2011). More specifically, the loss of articular cartilage occurs initially at the surface and then spreads down to the subchondral bone (Figure 5). The damaged cartilages always cause the development of pain, however the source of pain is still unclear, but it may be because of the inflammation of synovium (Vincent and Watt 2010).

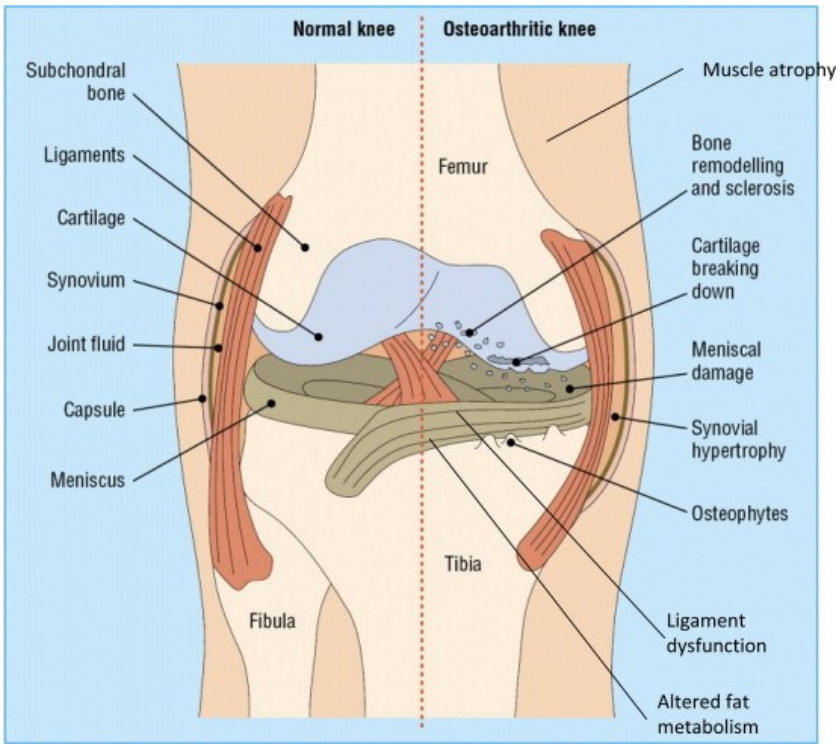

Figure 4. Comparison of normal knee with osteoarthritic knee (Hunter 2011)

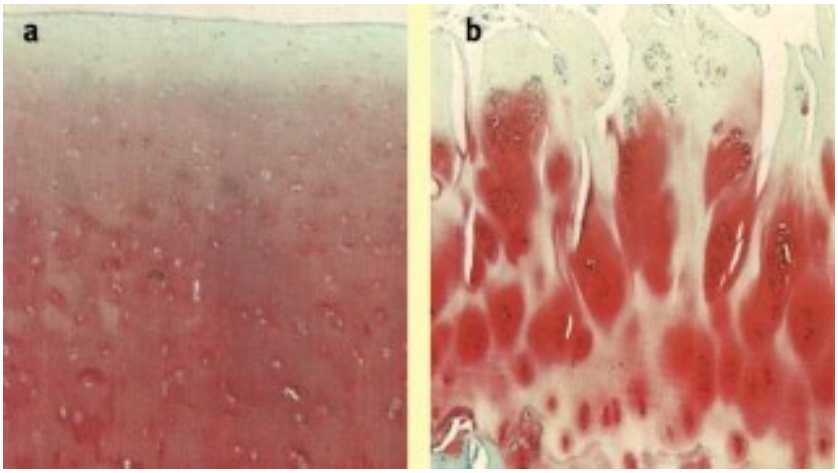

Figure 5. (a) Normal and **(b)** osteoarthritic human cartilage stained for proteoglycan (Vincent and Watt 2010)

There are several methods to diagnose OA such as self-report, radiography and blood tests. Self-report is a widely-accepted method. Inexpensive, easy to achieve, no needed to be trained for individuals collecting data and no additional health risks are the major advantages of OA case identification based on this way. However, the difficulty for individuals to identify the specific conditions is the main drawback of self-report method. Another method to identify the OA is called radiographic which has high internal validity because it forms part of the diagnostic criteria for OA. It has high inter- and intra-rater reliability. X-ray and other imaging modalities such as magnetic resonance and musculoskeletal ultrasound can be used to reflect the loss of volume of articular cartilage, but only X-ray is currently used for routine clinical assessment of OA; the other techniques are employed as research tools. However, the high cost of data collection and increased number of radiographs make this method become less encouraging (Busija *et al*. 2010). There is relatively new but tending to be normal method to identify OA based on blood tests. A modestly elevated C-reactive protein can be associated with 'erosive' OA in some patients. However, there is not reliable diagnosis and disease monitoring yet (Vincent and Watt 2010).

There are many possible risk factors which can be associated to OA such as age, excessive joint loading, sports participation, genetic factors, biomechanical factors and joint injury. The most important factor for all people is age. There is just less than 5% of people between 15 and 45 years old affected by OA, but the percentage increases to 25% to 30% among the people between 45-64 years old, and even to more than 60% or as high as 90% among the

people over 65 years old. The recent evidence shows that with the increasing age, the ability of cells to maintain and restore articular cartilages decreases, explaining why the percentage of people who has OA increases sharply with age (Buckwalter and Martin 2006). Another possible risk factor is excessive and repetitive joint loading. There is no study showing that normal daily activities and regular exercise can increase the risk of joint degeneration. However, the people whose occupation is about repetitive use of joint may have a higher risk to get joint degeneration. Also, some specific activities are associated to joint degeneration including lifting or carrying heavy objects very often. For example, female workers whose jobs are to pinch the thumb and index finger to hold something have a much higher rate of OA in the distal interphalangeal joints than other female workers (Felson *et al*. 2000). Obesity is a well-recognized high-risk factor in OA development. It is likely to result in an increased mechanical load on the weight-bearing joints, especially on the knee joint. Based on a large population-based survey, there is a strong relationship between high body mass index (BMI) and the risk of knee OA, and the people who are overweight has twice the risk of developing knee OA than people with normal weight. Participation in some competitive sports which demand high-intensity and direct joint impact, typically U.S. football, soccer and basketball, will increase the risk of the development of OA (Felson *et al*. 2000). Besides, the genetic factor cannot be ignored in the development of OA: 39-65% of OA is heritable. Biomechanical factors can be linked with OA including congenital hip dysplasia and unequal leg length. Joint injury in early life is also considered to be a factor of susceptibility to OA recently. The people who experienced joint injury in early life has a much higher risk of developing OA after 50 years than the normal people (Busija *et al*. 2010).

OA is not considered as a highly fatal disease, which means people with OA can live many years in a lasting state of disability; the morbidity is still prevalent, especially for the relatively old people. The morbidity associated to OA is largely attributable to the joints which bear most of the weight of bodies such as knees and hips (Busija *et al*. 2010). About one quarter of people over the age of 55 will suffer knee pain, and this number is higher in the older people (Peat *et al*. 2001). Although OA does not cause death directly, it will limit peoples' physical activity, athletic ability, and increase the risk of development of obesity. Some results of radiographic tests also show the trend that women with knee OA have a higher risk of death than general people (Busija *et al*. 2010).

The economic burden of OA in the old people cannot be ignored. OA is associated with an extremely high economic burden since it is the most common form of joint disease. OA costs more than 60 billion dollars per year in United States, and without considering pain effect and adverse psychosocial effect, it is estimated that job-related cost of OA are 3.4 to 13.2 billion US dollars per year, which means the job-related cost of OA is as much as job-related renal and neurological disease combined (Buckwalter and Martin 2006). Niskanen concluded that the cost due to radiological control per year in Finland was between 200 000 and 336 000 EUR (Niskanen, R.O. 2005). The economic burden includes indirect costs such as informal care and employment-related cost, and direct costs including medical treatment, and hospitalization and surgery costs (Gupta *et al*. 2005).

2.1.3 Osteoarthritis treatments

Traditionally there are three broad areas used to manage the OA patients which are lifestyle, medical and surgical interventions. Lifestyle treatment should be taught and kept all the time. Medical intervention is the first way to control the pain caused by OA. Surgical intervention is used when the medical treatments fail. In the lifestyle interventions, the management includes the effect of OA on patients' work, physical and leisure activities, function and quality of life. The patients should be educated to remain in work and exercise, to protect their body carefully and to be aware of the healthy diet in order to avoid the obesity. Also, all patients should be encouraged to keep physiotherapist's involvement. (Vincent and Watt 2010).

The non-surgical management of OA should be tried first. Basically, the pharmacological methods of OA can be divided into three categories: analgesics and non-steroidal anti-inflammatory agents (NSAIDs); symptomatic slow-acting drugs for osteoarthritis (SYSADOA); and disease-modifying osteoarthritis drugs (DMOADs). NSAIDs are always the first choice of osteoarthritis. Paracetamol is recommended to be the priority of self-medication by patients to treat osteoarthritis according to European League Against Rheumatism (EULAR) and Osteoarthritis Research Society International (OARSI) guidelines. It is also the most popular medical treatment for the relief of pain and inflammation. However, there are always some associations between NSAIDs and side-effects. Some patients who accept NSAIDs as the therapy develop ulcer disease. Also, the function of paracetamol is just to control the pain,

not primary care of the joints. DMOADs are now under development. Therefore, a SYSADOA like chondroitin sulphate is needed since it is a reliable candidate for the treatment of osteoarthritis (Kubo *et al*. 2009).

Surgical treatment is normally considered as the final option when the pharmacological procedures have failed to control the pain happened in the involved joints (Kubo *et al*. 2009). Restoring the degenerated articular surfaces is the core method of surgical treatment to OA. The damaged articular surface is restored with a new tissue which resembles but cannot duplicate the structure, composition and function of original articular cartilage. To repair degenerated articular surface with new tissue has become common in the recent five decades. The first and still the most commonly used method is the penetration of subchondral bone. However, after analysing the examination of joint surfaces by using arthroscopic abrasion, the results show that in some cases the formed fibrocartilaginous articular tissue contains little or no type II collagen. Also, it is not clear which kind of methods of penetrating subchondral bone can produce the best new articular surface. The difference of individuals, the age of patients and technique used during the surgery may cause different results. It has been recently reported that to decrease articular surface contact stress is an option to stimulate restoration of articular cartilage in OA joints. Another way is called soft tissue grafts which is a treatment of OA by debriding the joint and interposing soft tissue grafts consisting of fascia, joint capsule, muscle, tendon and periosteum between resected articular surfaces. This method can produce the best result in the younger individuals, which suggests that age may considerably affect the ability of undifferentiated cells to form an articular surface (Buckwalter and Martin 2006).

2.2 Polymers for the treatment of damaged cartilage

2.2.1 Traditional polymers studied for the treatment of damaged cartilage

In traditional surgical treatment, the damaged cartilage is always removed to decrease symptoms, which are usually shown as pain in joint, and to restore or maintain the normal functional articular surface. However, the result highly depends on the condition of the patient (Buckwalter and Mankin 1998). Currently, polymers used to treat damaged articular cartilage as in tissue engineering or directly to increase the lubrication has attracted a lot of

attention. However, most attempts to treat damaged articular cartilage have just focused on mimicking just one aspect of the cartilage properties which include mechanical resistance and lubrication in joints. Historically, the lubricating ability of cartilage tissue has been a secondary concern compared with the necessary mechanical properties. Therefore, the polymers synthesized to treat damaged cartilage should pass both mechanical and frictional properties (McNary *et al*. 2012). Besides, since the composition and organization of articular cartilage vary from the surface respect to the depth, the design and preparation of this tissue have remained challenging (Doulabi *et al*. 2014).

Polymers can be used as the matrix in tissue engineering to treat damaged cartilage. Both material and biological requirements of the polymer should be considered for the tissue engineering application. The polymer should be biocompatible and non-toxic, and it should have a desired degradation rate, surface property, processability, porosity, and mechanical properties. For the biological side, the immunogenic and foreign body reactions should be avoided (Kim *et al*. 2011).

Synthetic materials such as poly(lactic acid) (PLA), poly(glycolic acid) (PGA), and poly(lactic acid-co-glycolic acid) (PLGA) have been studied for cartilage tissue engineering since they are easy in molding and controlling the desired degradation rate to match tissue growth. However, an inflammation reaction may be caused because of the acidic by-products generated during the degradation process. Also, these materials cannot attach to the joint tissue effectively. Hence, these synthetic materials are not preferred for cartilage tissue (Kim *et al*. 2011).

Balasundaram *et al* synthesized a kind of nanoembossed polyurethane (NPU) and nanoembossed polycaprolactone (NPCL) which have a highly porous surface with nanoscale roughness. The results showed that both NPU and NPCL possessed higher nanoscaled surface roughness and surface energy compared with the original polymers, and an increase in chondrocyte numbers on NPU and NPCL compared with their respective plain polymers after periods of up to 7 days was observed. They suggested that these materials may be suitable for numerous polymer-based cartilage tissue-engineering applications (Balasundaram *et al*. 2014).

Hydrogels with very high water content (e.g. 90 wt%) are used in cartilage tissue engineering

to carry cells or biomechanical tissue replacements, but they must be combined with other polymers to produce strong enough materials (Liao *et al*. 2013). Polyvinyl alcohol (PVA) is a type of synthetic polymer derived from polyvinyl acetate. PVA hydrogels have been investigated for the treatment of damaged cartilage due to its high-water content and excellent mechanical properties (Baker *et al*. 2012, Stammen *et al*. 2001). Polyvinylpyrrolidone (PVP) is another hydrogel that has been used in biomedical applications due to its high hydrophilicity (Ma *et al*. 2009). Shi and Xiong synthesized PVP/PVA hydrogels and investigated the effect of different experimental conditions including polymerization degree of polyvinyl alcohol, polymer concentration, lubrication condition (dry, physiological saline, and bovine serum) and the load on the friction properties of PVA/PVP hydrogels. The results showed that the lubrication conditions and the applied load were the primary factors to affect the friction coefficient, while the effect of PVA polymerization and polymer concentration were negligible. When bovine serum lubrication was applied, the friction coefficient was the smallest one (Shi and Xiong 2013). However, the PVA/PVP hydrogels cannot mimic the whole functions of real articular cartilage since the structure and composition of articular cartilage are complex, and the durability of PVA/PVP needs to be studied. Experiments in *vivo* were not evaluated; nevertheless, the adherence of the material to host cartilage tissues is a critical issue if the PVA/PVP hydrogel is going be used for the replacement of articular cartilage. On the other hand, Wathier *et al*. reported that poly(7-oxanorbornene-2-2carboxylate) is a good lubricant for articular cartilage. After modifying the molecular weight and concentration, the polymer (2.5 MDa, 2% w/v) reduced the friction like synovial fluid. However, how to ensure that the polymer can stay on the surface of cartilage was not discussed, and additional *in vivo* tests to further evaluate its performance must be accomplished (Wathier *et al*. 2013).

Hydrogels of naturally derived polymers (proteins or polysaccharides) such as fibrin, peptide, collagen, chitosan, agarose and alginate are being studied for the treatment of damaged cartilage. Chitosan is used in cell transplantation and tissue regeneration because it is structurally like the glycosaminoglycans found in cartilage (Spiller *et al*. 2011), and it is enzymatically degraded *in vivo* by lysozyme which is present in human cartilage (Park *et al*. 2013). In addition, chitosan can show excellent ability to be processed into porous structures (Suh and Matthew 2000). Park *et al*. synthesized chitosan composite hydrogels which

contained hyaluronic acid (HA) for the treatment of cartilage defects. They investigated the effect of HA on biological properties of chitosan composite by analysing the results of the morphology, gelation time, mechanical strength and degradation of chitosan hydrogels with different initial conditions. The chitosan hydrogels showed good cytocompatibility, and cell proliferation and cartilaginous ECM were considerably increased with the existence of HA (Park *et al*. 2013). Because agarose and alginate are easy to gelate and encapsulate, they are popular for the production of hydrogels, which are available commercially (Spiller *et al*. 2011). However, general drawbacks of hydrogels made of natural polymers are poor mechanical property and possibility for disease transmission through material derived from animals, which limit the practical application of this type of hydrogels.

Cellulose nanofibrils (CNF) is a promising material used in biomedicine not only because of its remarkable mechanical property, but also its biocompatibility, natural origin and abundance. Valle-Delgado *et al*. prepared a highly lubricating CNF film by attaching hyaluronic acid on the surface, which was proposed as a potential candidate for cartilage replacement (Figure 6). The experiments with a model system show a considerable reduction in the friction force and friction coefficient of CNF films after attaching HA. In particular, HA decreased the friction coefficient between 60% and 90% at different pH and ionic strength. The larger the swelling of the HA layer, the better the lubrication was (Valle-Delgado *et al*. 2016). However, the performance of the material in a real cartilage and the mechanism for proper fixation in the joint need to be studied further.

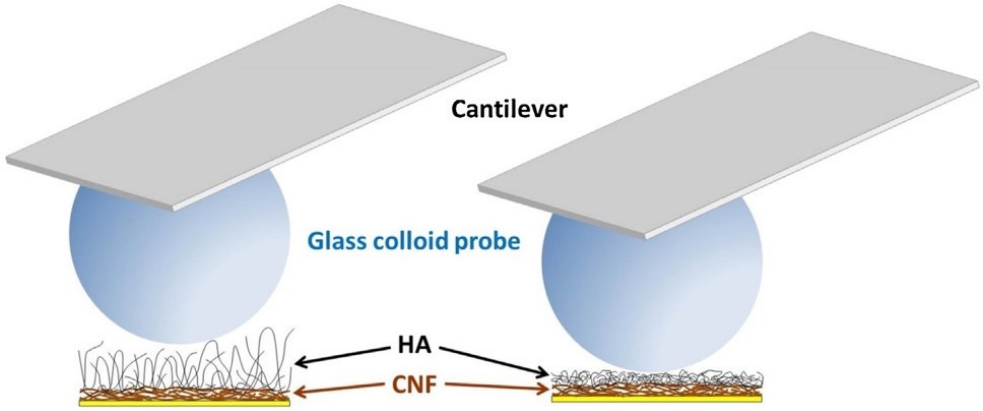

Figure 6. CNF-HA films at high pH and low ionic strength (left) and at low pH and high ionic strength (right) (Valle-Delgado *et al*. 2016).

A new approach based on brush-like polymer has attracted lots of attention. Morgese *et al*. have experimentally proved that both linear and cyclic brushes can provide lubrication, and the cyclic brushes show a "super-lubricating" behavior due to its distinctive features including higher steric stabilization than linear brushes and high grafting density (Morgese *et al*. 2016). This notion has inspired the use of synthetic brush-like polymer as boundary lubricants to reduce the boundary friction between cartilages (Morgese *et al*. 2017, Samaroo *et al*. 2017). Morgese *et al*. synthesized a type of brush-like polymer using poly(glutamic acid) (PGA) as backbone and poly(2-methyloxazoline) (PMOXA) as the side chains. Aldehyde groups were introduced to increase the attachment between the cartilage and polymers. The friction results show that polymers with relative higher grafting density and shorter chain length could provide better lubricating ability under high loading, while the polymers with lower grafting density and shorter chain length showed the best lubricating behaviour when the applied load is lower. Based on the advantages of great lubricating ability, high biocompatibility and *in vivo* stability, they consider this polymer as a promising candidate to treat OA. However, further experiments should focus on the biomechanical properties of this type of brush-like polymer (Morgese *et al*. 2017).

Poly(L-lysine)-graft-poly(ethylene glycol) (PLL-g-PEG) is a copolymer consisting of a poly(L-lysine) backbone and polyethylene glycol side chains which can reduce the coefficient of friction under both sliding conditions and rolling conditions. Drobek and Spencer reported the investigation of tribological properties of PLL-g-PEG films, in which PLL-g-PEG showed considerable low friction when shear was applied, and the layer thickness of copolymer depended on the length of PEG side chains, adsorption conditions and surface concentration of adsorbed molecules. However, since many practical conditions in articular cartilage tissue were not considered in the experiments, further studies are needed to check the potential of PLL-g-PEG films for cartilage treatment (Drobek and Spencer 2008). By changing the backbone of the brush-like polymer from PLL to polyacrylic acid(PAA), Samaroo *et al* synthesized a library of PAA-g-PEG copolymers with controlled hydrodynamic size through varying the backbone lengths, brush sizes and brush densities (Figure 7) to mimic the brush-like structure of the natural glycoprotein lubricin and its binding and lubricating abilities. The results showed that the brush-like polymers could bind to cartilage surface effectively, and the bound lubricants reduced the friction successfully. To be specific, larger molecules take longer to

bind to the cartilage surface. It took longer time for polymers with larger PAA backbones, PEG brushes, and PEG: AA brush densities to bind. However, the results did not show a clear relationship between polymer structure and lubricating ability. Further, the binding strength may not be strong enough; the polymer might be pushed away when large load or motion are applied since the binding is not covalent (Samaroo *et al*. 2017).

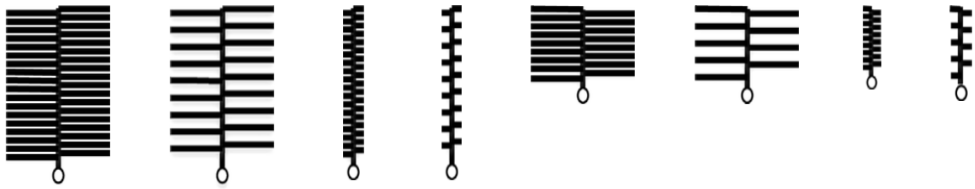

Figure 7. PAA-g-PEG with different backbone length, brush size and brush density (Samaroo *et al*. 2017).

2.2.2 New strategy for the treatment of damaged cartilage: carboxymethyl cellulose (CMC) and polyethylene glycol grafted carboxymethyl cellulose (CMC-g-PEG)

A brush-like polymer based on CMC can be employed to give good lubrication by binding it to collagen in the cartilage. Therefore, it is essential to know the basic CMC chemistry. Cellulose is the most abundant biopolymer on earth, but most of the cellulose is used in paper production (El-Sakhawy *et al*. 2014). However, cellulose is attracting more and more attention in the area of chemicals because of the increasing demand for environmentally friendly and biocompatible products (Chang and Zhang 2011). CMC is a very important hydrophilic biocompatible polymer, derived through etherification of cellulose (Habibi 2014). Figure 8 shows schematically how CMC is prepared from the reaction of cellulose with chloroacetic acid. Due to the presence of carboxyl groups, CMC is a negatively charged polymer soluble in water (Gaihre and Jayasuriya 2016). CMC has been produced commercially since the early 1920's (Ogushi *et al*. 2007), and now is the most widely used cellulose derivative (Oun and Rhim 2015). Due to its unique properties such as high viscosity, transparency, hydrophilicity, non-toxicity, biocompatibility, moisture sorption property (Yadav *et al*. 2013) and biodegradability, CMC has been employed for many applications including drug delivery, dermal tissue engineering (Ninan *et al*. 2013), textile printing, detergents, food industry (Yadollahi *et al*. 2014) and preparation of hydrogels.

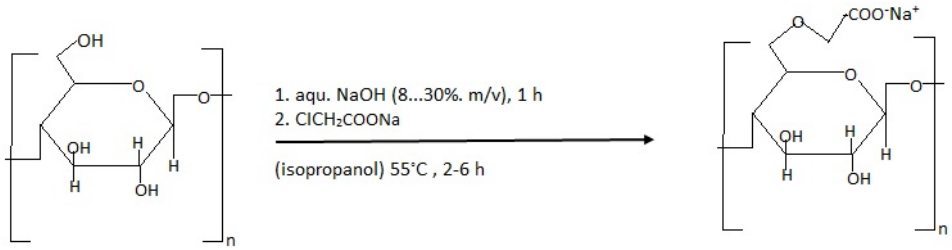

Figure 8. Schematic figure of the preparation of CMC (modified from Heinze and Pfeiffer 1999).

CMC has been used for biomedical applications for a long time. Jiang *et al*. synthesized nano-hydroxyapatite/chitosan/CMC composite scaffolds to solve the problems of poor interconnected porous structure and cytotoxicity from the residue salt particles happened in nano-hydroxyapatite/chitosan composites. Scaffolds with good porous structure, high compressive strength, acceptable degradation rate and good bioactivity were produced by adding the appropriate percentage of CMC, and they are a promising material in the field of bone repair (Jiang *et al*. 2008). Drug delivery is another application of CMC. Ugwoke *et al*. formulated an apomorphine delivery system using CMC as the polymeric carrier and characterized it with respect to *in vitro* and *in vivo* drug release (Ugwoke *et al*. 2000). Shiow-Fern and Nafisah developed a kind of carboxymethyl cellulose lyophilised wafers that contained antimicrobials intended for wound infections. The Na-CMC wafer showed desired flexibility, sponginess, uniform wafer texture, white colour and acceptable odour (Shiow-Fern and Nafisah 2014). Chang *et al*. also prepared a kind of superabsorbent hydrogel using cellulose as the backbone and CMC as hydrophilic filler in NaOH/urea aqueous system. They measured the swelling properties, salt sensitivities, and the prolonged protein release behaviours of the hydrogel. The results showed that this type of hydrogel exhibited superabsorbent capacity and controlled equilibrium swelling ratio by changing the amount of CMC. Furthermore, the hydrogel showed smart swelling and shrinking behaviours in inorganic salts aqueous solution, physical saline water and synthetic urine. The release time of bovine serum albumin could be controlled by changing the content of CMC. This hydrogel has potential applications in the biomaterial field (Chang *et al*. 2010).

Brush-like molecular architectures (Figure 9) are well-known in biology, and this kind of unique structure has inspired the synthesis of polymers with similar architectures. For

instance, the lubricin which is the primary boundary lubricant of articular cartilage is a type of brush-like molecule. It is responsible for the significant boundary lubrication mechanisms, and facilitate the generation of repulsive forces between apposing cartilage surfaces. The properties of brush-like polymers do not only depend on the architecture of the backbone, but also on the length, density and stiffness of the side chains. However, the greatest effect on properties and conformation are achieved when the side chains are densely grafted (Peleshanko and Tsukruk 2008). The key mission of this kind of brush-like material in the application of cartilage treatment is to ensure the grafted polymer can effectively increase the lubrication between cartilages.

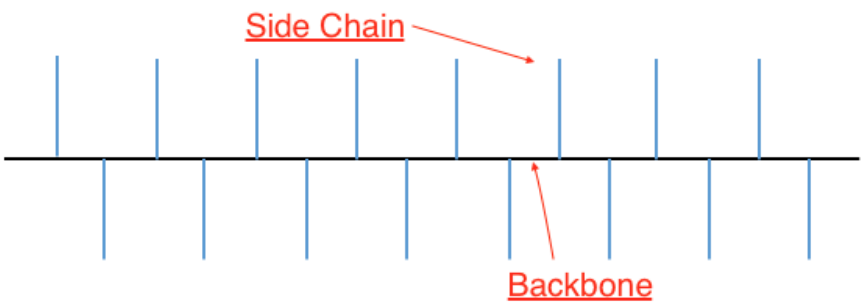

Figure 9. Architecture of brush-like polymer

Polyethylene glycol (PEG) is a synthetic polyether used in a wide range of molecular weights. This polymer is amphiphilic and soluble in water and in many organic solvents such as ethanol, acetone, toluene and chloroform (Kono, H. 2014). Since there is a hydroxyl group at the end of the PEG chain, the polymer can be easily functionalized with many other functional groups. PEG and CMC have been employed together in the biomedical application field. Lee *et al*. synthesized PEG-CMC hydrogels and observed that their properties such as gel point, swelling behaviour, degradation and protein release rate were affected by the content of CMC. Further, this PEG-CMC gel had the potential application of pH-sensitive drug carrier (Lee *et al*. 2016). PEG is a promising polymer to modify surfaces since it can simultaneously impart biocompatibility and lubricity to materials (Chawla *et al*. 2009).

PEG grafted at the polymer backbone has also been shown the ability to increase lubrication

between solid surfaces in aqueous solutions, and such aqueous lubrication is especially important in biomedical applications (Olszewska *et al*. 2013a, Drobek and Spencer 2008). Brush-like polymers with PEG side chains have also been studied as possible candidates for the treatment of injured cartilage (Samaroo *et al*. 2017). CMC is a possible choice acting as the backbone to synthesize the brush-like polymers. Some reports have also discussed the possibility of using CMC as the backbone and PEG as the brush to increase the lubricating ability of the polymer. Olszewska *et al*. used polyethylene glycol-grafted carboxymethyl cellulose (CMC-g-PEG) as the boundary lubricant to reduce the friction between cellulose nanofibrils. The results indicated that the lubricating effect of CMC-g-PEG is strongly pH dependent. Drastically reduced friction was observed at pH 7.3, while only moderate friction reduction was noted at lower pH. Compared with CMC-g-PEG which reduced the friction by 65% and 88% at pH 4.5 and pH 7.3, respectively, the reduction in friction by only CMC was just 13% and 22% for the respective pHs. Those observations provided the evidence for the good lubricating ability of CMC-g-PEG (Olszewska *et al*. 2013a). Olszewska *et al*. also reported a good lubrication in the air between cellulose surfaces with adsorbed CMC-g-PEG (Olszewska *et al*. 2013b).

Greene *et al*. described a system which can simulate fluid pressurization mechanism and boundary lubrication mechanism by adsorbing CMC-g-PEG on a cellulose fibre network used to mimic the structure, mechanical properties and fluid transport properties of articular cartilage tissue (Figure 10). The results show that this system can reduce the friction forces through the pressurization of interstitial fluid as well as through the boundary lubrication of CMC-PEG, indicating that this system could be used in the areas of implantable materials. However, there are still some disadvantages such as uneven pore size distribution and permeability which need to be tackled to improve the system, as well as poor mechanical properties, which means that material was not tough enough for most practical applications (Greene *et al*. 2014).

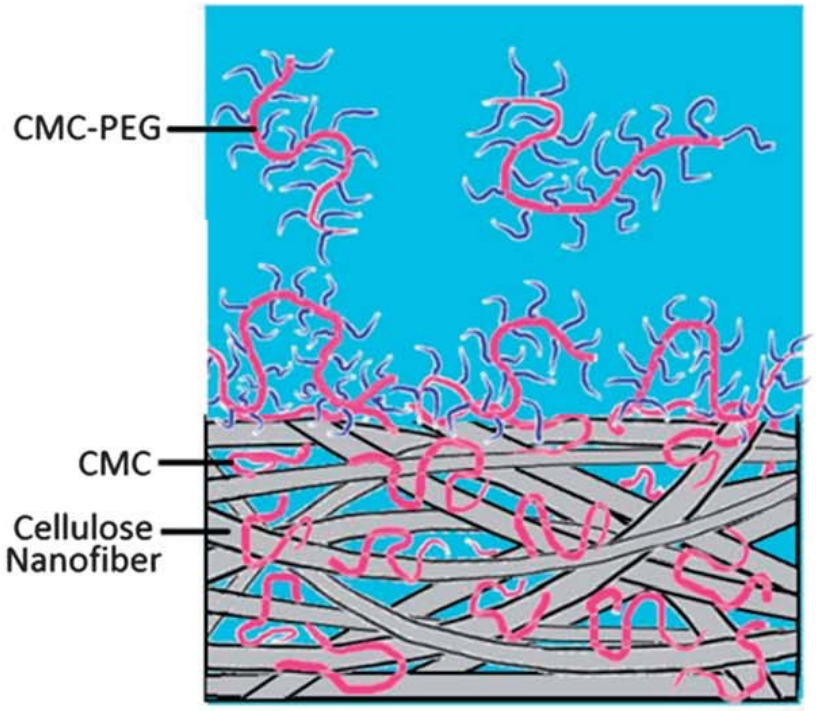

Figure 10. Schematic illustration of a cellulose nanofiber network modified by adsorption of CMC and CMC-PEG (Greene *et al*. 2014).

This MSc thesis project aims to advance on the potential application of the lubricating CMC-g-PEG for the treatment of damaged cartilage. Two PEGs with different molecular masses were used in the preparation of CMC-g-PEG in this project. In order to enhance the binding of the polymer to cartilage, CMC-g-PEG was modified by introducing aldehyde groups to the CMC backbone.

2.2.3 Dialdehyde carboxymethyl cellulose (DCMC)

Periodate oxidation has been employed in the industry for a long time. Dialdehyde polysaccharides have received a great deal of attention as an ideal crosslinking agent. For example, dialdehyde starch prepared by introducing aldehyde groups in starch has been used as a crosslinker to prepare a 3D spongy collagen cryogel (Mu *et al*. 2012). Hua *et al*. also showed the possibility of crosslinking collagen and alginate dialdehyde (ADA) because of the existence of aldehyde groups in ADA and amino groups within collagen molecules (Figure 11) (Hua *et al*. 2014). It has been reported that dialdehyde polysaccharides can be used to

crosslink gelatin (a derivative of collagen) through the C=N linkages between aldehyde groups in dialdehyde polysaccharides and 3-amino groups of lysine or hydroxylysine side groups of gelatin (Figure 12) (Mu *et al*. 2012). In the area of derivatization of cellulose, periodate oxidation is a promising method to convert dihydroxyl groups to dialdehyde groups so that the derived cellulose can be used in further reactions. The periodate oxidation of cellulose is a highly specific reaction to convert 1, 2-dihydroxyl groups to dialdehyde groups (Teotia, A. 2012). CMC, as well as cellulose, is partially oxidized by sodium periodate through specifically cleaving the C_2-C_3 bond of the 1, 4-glucan unit to form dialdehyde carboxymethyl cellulose (DCMC) (Figure 13) (Wang *et al*. 2015). Aldehyde groups can be further converted to carboxylic acids, primary alcohols or imines with primary amines, which brings dialdehyde cellulose the opportunity to act as a useful intermediate for many cellulose-based functional materials such as drug carriers or substrates for the separation and analysis of proteins (Li *et al*. 2011).

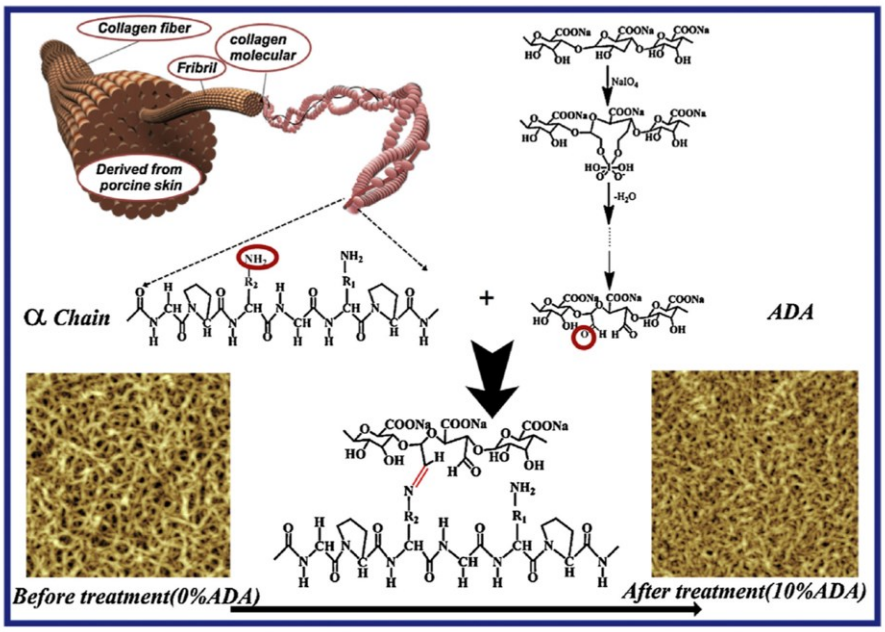

Figure 11. Interactions between collagen and alginate dialdehyde (Hua *et al*. 2014).

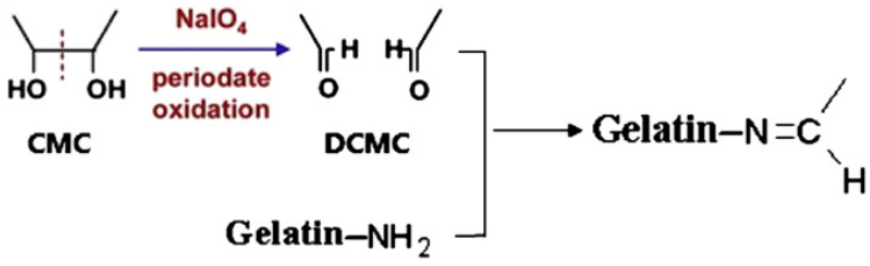

Figure 12. Crosslink between DCMC and Gelatin (Mu *et al*. 2012).

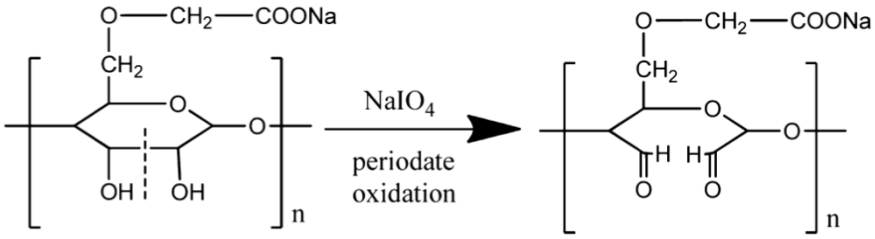

Figure. 13 Preparation process of DCMC (Wang *et al*. 2015).

With the aim of developing a lubricating polymer with potential application for cartilage treatment, in this work, CMC-g-PEG was oxidized with sodium periodate to get DCMC-g-PEG, whose aldehyde groups are expected to bind covalently to the amine groups of collagens in cartilage.

2.3 Quartz crystal microbalance with dissipation monitoring (QCM-D)

QCM-D was used to study the adsorption of polymers on the surface of collagen films in this project. Quartz was the first piezoelectric material to be widely used. Traditional Quartz Crystal Microbalance (QCM) is a simple, cost-effective, high-resolution technique, and has been used for more than 50 years to analyze mass changes on rigid surfaces, most effectively in air or vacuum (Marx, K.A. 2003). QCM was initially used as a mass detector in vacuum or air, but later it has been used in many fields such as biology, surface analysis, physics, polymer science and environment science after scientists found that QCM may also be used in the liquid phase. Quartz Crystal Microbalance with Dissipation monitoring (QCM-D), developed

in 1995 (Rodahl *et al.* 1995), is a real-time, nanoscale technique for analyzing surface phenomena including thin film formation, adsorption and reactions, and more and more scientific reports using this technique have been published in the last decade (Liu and Zhang 2013).

The principle of QCM-D can be briefly described as monitoring the frequency and energy dissipation response of a freely oscillating sensor during the adsorption of any material on its surface. Figure 14 shows the main components in QCM-D. The resonance frequency (*f*) of the sensor depends on the total oscillating mass. When a thin and rigid film is attached to the sensor, the decrease in frequency is proportional to the mass of the film. The mass of the adhering layer is calculated through the Sauerbrey equation (Sauerbrey, G. 1959):

$$\Delta m = -\frac{C \cdot \Delta f}{n} \qquad (1)$$

Where *C* is a constant that depends on the thickness of quartz, *f* is the resonance frequency, *n* is the overtone number and *m* is the mass of the film (Czandema and Lu 1984).

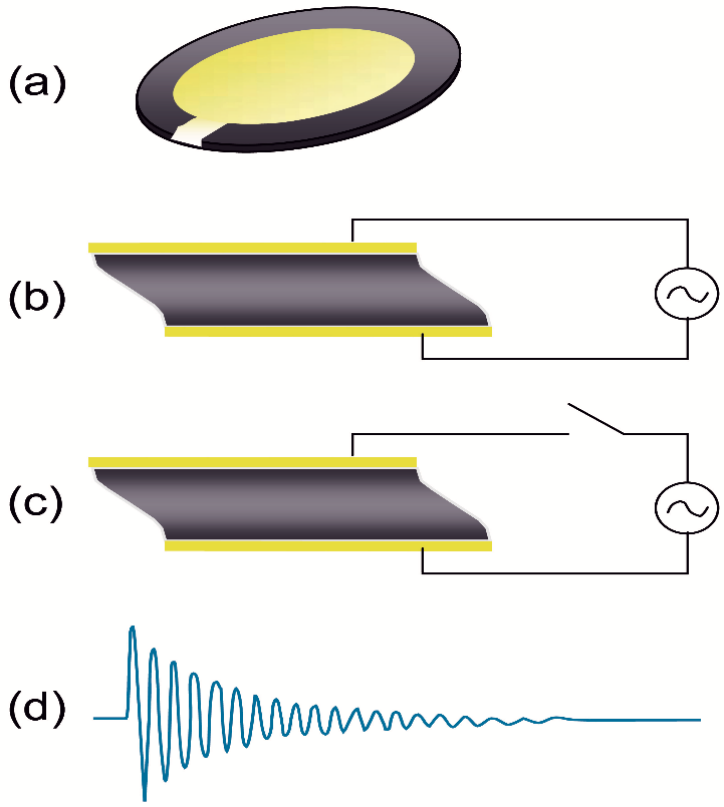

Figure 14. The main components in QCM-D. **(a):** Typical QCM-D sensor with Au electrodes. **(b):** Quartz crystal oscillating when an alternating current is applied across electrodes. **(c):** Interruption of electrical excitation. **(d):** The oscillatory decay as the quartz disk comes to rest (Dixon 2008).

However, in most cases, the adsorbed film is not rigid which means the Sauerbrey equation is not valid, and it will underestimate the mass at the surface when a viscoelastic film is attached to the sensor. Therefore, the Johannsmann's equation (Johannsmann *et al.* 1992) is used for more accurate estimate of the true sensed mass for viscous films:

$$\hat{m}^* = m^0(1 + \hat{J}(f)\frac{\rho f^2 d^2}{3}) \qquad (2)$$

where $\hat{m}^*$ is the equivalent mass, ρ is the density of the fluid, d is the thickness of the film, $\hat{J}(f)$ is the complex shear assumed independent of frequency, and m^0 is the true sensed mass. The latter is obtained from the intercept of a plot taking the equivalent mass as the function of frequency squared (Eronen *et al*. 2011).

The viscoelasticity of the adsorbed layer can be detected by the energy dissipation (D) of the sensor's oscillation (Modin et al. 2006). The energy dissipation of the sensor is measured by

recording the response of a freely oscillating sensor that has been vibrated at its resonance frequency when the driving voltage is shut off. *D* is defined as:

$$D = \frac{E_{lost}}{2\pi E_{stored}} \quad (3)$$

Where E_{lost} is the energy dissipated during one oscillation cycle and E_{stored} is the total energy stored in the oscillator. By measuring at multiple frequencies and applying a viscoelastic model, some properties such as viscosity, elasticity and thickness of soft films can be characterized in detail.

QCM-D simultaneously measures the mass and viscoelasticity on a material surface. Due to the high sensitivity in the range of ng/cm^2 in liquid phase measurement, the dynamic behaviour of brush-like polymer can be studied on nanoscale, which means by using the QCM-D technique, it is possible to evaluate the water absorption in the polymer brush layers and the viscoelasticity of the polymer-hydrated layers in water. Kitano *et al*. synthesized nanoscale poly(2-methacryloyloxyethyl phosphorylcholine), poly(2-hydroxyethyl methacrylate) and poly(methyl methacrylate) brush layers and investigated the effect of hydration of brush layer on resistance to friction by analysing the dynamic behaviour of brush layer with the help of QCM-D (Kitano *et al*. 2009). Similarly, with the use of QCM-D, Slavin *et al*. studied how oligo(ethylene glycol) chains affected the adsorption behaviour of sulfur groups when sulfur-containing polymers attached on the surface of gold (Slavin *et al*. 2012). Successful characterization of biomolecular systems in their natural aqueous environment is the important objective of biosensoring. QCM operating in fluids offers such straightforward possibility (Voinova *et al*. 2002). Besides the advantages of the measurement of both mass and viscoelastic properties of adsorbed films, another major advantage of QCM-D is the flexibility in the choice of substrate. Any material that can be evaporated or deposited within a sufficiently thin regime is capable of being coated on the QCM-D surface, which means surfaces can be monitored stepwise during preparation and used as sensor platforms to study further biomolecular interactions. A number of biologically relevant applications of the QCM-D including biosensor, monitoring and characterization of biofilm deposition, biomolecule binding kinetics, and some biomolecular studies with DNA, cells, lipids and proteins have been reviewed in the literature (Dixon 2008, Ferreira *et al*. 2009).

QCM-D has also been vastly employed in studies related to cellulose. Eronen *et al*. studied the adsorption behaviour of water-soluble polysaccharides or cellulose derivatives to nanofibrillar cellulose films in order to compare how the basic chemical composition and molecular weight of polysaccharides affect the interactions and surface properties of the films. The results showed that xyloglucan had the highest adsorption rate on the nanofibrillar cellulose film and the highest adsorbed amount in the initial stage of adsorption. Neutral, degraded guar gum and CMC with anionic charge showed similar trend in dissipation, but the adsorbed mass of guar gum was higher than CMC. Chitosan could adsorb very fast at pH 4.5, but the adsorbed mass was quite low since very small amount of chitosan was needed for charge neutralization of nanofibrillar cellulose. The adsorption behaviours of differently structured anionic polysaccharides were similar on nanofibrillar cellulose substrates. Therefore, neither cellulose supramolecular structure nor hemicelluloses present in the nanofibrillar cellulose film affected the adsorption of anionic polysaccharides (Eronen *et al*. 2011). Olszewska *et al*. also used QCM-D to study the adsorption of CMC-g-PEG on nanofibrillar cellulose. They found that the adsorbed amount of CMC-g-PEG was slightly smaller than the reference CMC, but their adsorption kinetics and the change in dissipation were quite similar. The results indicated that both CMC and CMC-PEG retained their own swollen state which is considered as a major advantage in lubrication applications, and the adsorption of CMC and CMC-g-PEG did not affect the morphology of nanofibrillar cellulose films (Olszewska *et al*. 2013a).

In this project, QCM-D has been used to investigate the adsorption properties of CMC-g-PEG and DCMC-g-PEG on the surface of collagen films (a model system for cartilage surface).

3. Experimental

3.1 Materials

All the chemicals used in this project were of analytical grade. Sodium acetate trihydrate ($CH_3COONa*3H_2O$, VWR), glacial acetic acid (CH_3COOH, Emparta) and distilled water were used to prepare acetate buffer solution. Hydrochloric acid (HCl, 1 M and 0.1 M, Merck Millipore) and pH meter (Mettler Toledo) were used to adjust the pH of acetate buffer to 4.5.

Carboxymethyl cellulose (Na-CMC, 250,000 g·mol^{-1}, DS 0.70, Sigma-Aldrich), 1-ethyl-3-(3-dimethylaminopropyl) carbodiimide hydrochloride (EDC, Novabiochem), N-hydroxysuccinimide (NHS, Sigma-Aldrich) and methoxy polyethylene glycol amine (OMe-PEG-amine, 2 kDa and 5 kDa, Nanocs) were used to synthesize CMC-g-PEG. Sodium hydroxide (0.1 M NaOH, Merck Millipore) and sodium chloride (NaCl, Oy FF-Chemicals Ab) were used to titrate CMC-g-PEG. Potassium bromide (KBr, Fluka) was used in FTIR measurements. Sodium periodate ($NaIO_4$, Sigma-Aldrich) was used to synthesize DCMC-g-PEG. Collagen IV from human placenta (Sigma-Aldrich) was used to test polymer adsorption in phosphate buffered saline (PBS, Sigma-Aldrich) by QCM-D.

3.2 Methods

3.2.1 Synthesis of CMC-g-PEG and DCMC-g-PEG

CMC was dissolved in ultrapure MilliQ water and the solution was stirred overnight to ensure the complete dissolution of CMC. The solution was then dialyzed using a dialysis tube (regenerated cellulose, 12-14 kDa, Spectra/Por) against ultrapure MilliQ water for four days to remove the low molecular weight CMC and then freeze-dried (FreeZone 2.5, Labconco). Following the procedure described by Olszewska *et al*. (Olszewska *et al*. 2013a), 250 mg freeze-dried CMC was dissolved in 125 ml buffer 10 mM NaAc/HAc pH 4.5 (12.5 ml 100 mM NaAc/HAc + 112.5 ml MilliQ water) and then mixed overnight. Subsequently, 479.84 mg of EDC and 1152.33 mg of NHS were mixed into the CMC solution and stirred for 1.5 h to allow EDC and NHS to fully react with CMC. 251.11 mg of OMe-PEG-amine (2 kDa) was then added to the solution. The reaction took place at room temperature for 24 h by stirring in a sealed beaker to synthesize CMC-g-PEG. Figure 15 illustrates the synthesis of CMC-g-PEG. The CMC-g-PEG solution was dialyzed against ultrapure MilliQ water in order to remove unreacted PEG, and then the solution was freeze-dried again to get the solid sample. To evaluate the effect of PEG chain length on the properties of CMC-g-PEG, OMe-PEG-amine (5 kDa) was also used to prepare CMC-g-PEG. The preparation process of CMC-g-PEG was same, but the amount of OMe-PEG-amine (5 kDa) used in the reaction were 500.30 mg. Further, the reaction took place for 30 h to give more time to the longer PEG chain to graft to the CMC backbone. To clarify in the thesis, the CMC-g-PEG is written as CMC-g-PEG (2) when OMe-PEG-amine (2 kDa)

was used during the reaction, and CMC-g-PEG (5) means it was synthesized using OMe-PEG-amine (5 kDa).

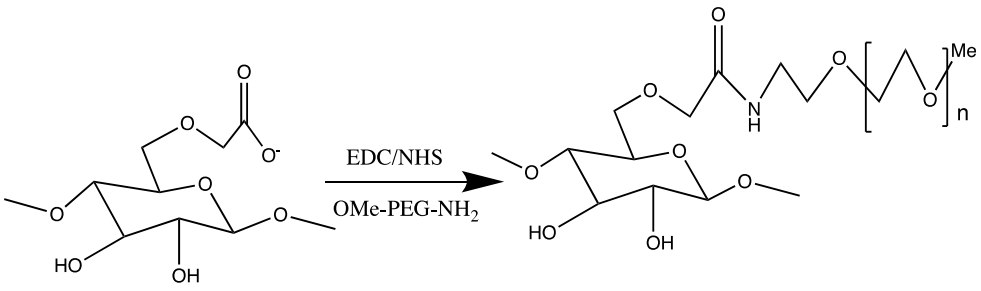

Figure 15. The synthesis of CMC-g-PEG (Olszewska *et al.* 2013a).

The synthesized CMC-g-PEG (2) and CMC-g-PEG (5) were transformed into DCMC-g-PEG (2) and DCMC-g-PEG (5) based on the protocol described by Li *et al.* (Li *et al.* 2011). 101.47 mg of CMC-g-PEG (2) was dissolved in 20 ml ultrapure MilliQ water at room temperature. In order to achieve $NaIO_4$/CMC-g-PEG (2) molar ratio 1:1, 58.70 mg of sodium periodate was dissolved in 10 ml ultrapure MilliQ water, which was then added to the CMC-g-PEG (2) solution under stirring. The pH was adjusted to 3 with 0.1 M hydrochloric acid. The mixed solution was stirred in dark environment at 35 ˚C for 6 h. The solution was then dialyzed against ultrapure MilliQ water and freeze-dried to get solid DCMC-g-PEG (2). The same procedure was applied to synthesize DCMC-g-PEG (5) from 96.66 mg of CMC-g-PEG (5) and 58.20 mg of $NaIO_4$. Figure 16 illustrates the synthesis of DCMC-g-PEG.

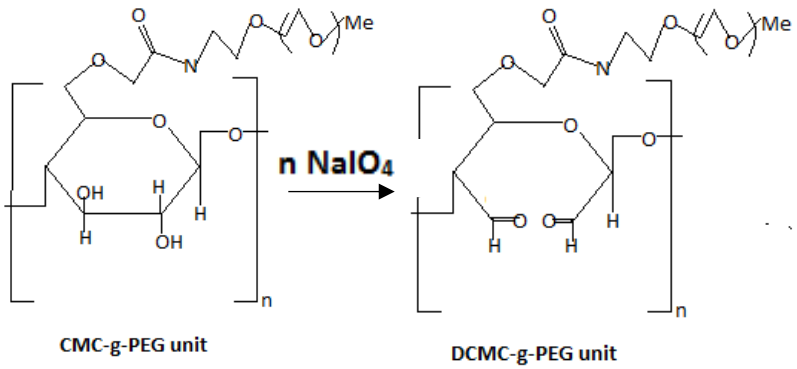

Figure 16. The synthesis of DCMC-g-PEG (Modified from Li *et al*. 2011).

3.2.2 Characterization of CMC-g-PEG by conductometric titration

Direct polyelectrolyte titration was used to determine the number of unsubstituted carboxyl groups after synthesis of CMC-g-PEG. 25.46 mg dialyzed CMC was dissolved in 500 ml ultrapure MilliQ water. 1 ml sodium hydroxide (0.1 M) and 0.5 ml sodium chloride (0.1 M) were then added to the solution. The solution was titrated by adding fix amounts of hydrochloric acid (0.01 M) with a dispenser. The conductivity of the solution was recorded (conductometer CG 855, Schott) as a function of the amount of hydrochloric acid added. The same amount of CMC-g-PEG and titration processes were used to titrate CMC-g-PEG (2) and CMC-g-PEG (5).

The three phases of the conductometric titration curve were fitted linearly to analyse the charge of the sample. The volume of hydrochloric acid needed to titrate the carboxyl groups of polymers are given by the difference between V_2 and V_1. V_2 and V_1 can be calculated from the intersection of the fitting lines. The charge *X* of the dialyzed CMC or CMC-g-PEG were calculated in micromoles of hydrochloric acid per gram of dialyzed CMC or CMC-g-PEG (µmol/g) from the equation:

$$X=\frac{C(V_2-V_1)}{m} \qquad (4)$$

Where X is the total carboxyl group content, in µmol/g; C is the concentration of hydrochloric acid solution; V_2 is the volume of the hydrochloric acid solution consumed at the second intersection point; V_1 is the volume of the hydrochloric acid solution consumed at the first intersection point; and m is the weight of dialyzed CMC or CMC-g-PEG.

3.2.3 Characterization of CMC-g-PEG and DCMC-g-PEG by FTIR

Fourier transform infrared (FTIR) spectra of dialyzed CMC, CMC-g-PEG (2), CMC-g-PEG (5), DCMC-g-PEG (2) and DCMC-g-PEG (5) were obtained from discs which contained about 5 mg of dry sample in 300 mg potassium bromide (KBr). The measurements were recorded by FTIR spectrophotometer (Thermo Electron Corporation) at the resolution of 4 cm^{-1} in the wave number region 500-4000 cm^{-1}. All the FTIR spectra of polymers were analysed according to the infrared absorption table available in the link:

https://chem.libretexts.org/Reference/Reference_Tables/Spectroscopic_Parameters/Infrared_Spectroscopy_Absorption_Table.

3.2.4 Adsorption of DCMC-g-PEG and CMC-g-PEG on collagen IV films studied by QCM-D

In order to investigate the attachment of DCMC-g-PEG and CMC-g-PEG to collagen IV, the gold sensors (QSX 301) were cleaned with nitrogen and then coated with collagen IV using the spin coater (Laurell, WS-650SX-6NPP/LIITE) for 1 min at 4000 rpm. CMC-g-PEG and DCMC-g-PEG were dissolved in PBS buffer respectively to prepare the polymers solution with a concentration of 100 µg/ml or 1 mg/ml. The attachment of DCMC-g-PEG and CMC-g-PEG to collagen IV films was monitored by QCM-D (E4, Q-Sense AB, Sweden). All measurements were performed at 25 ˚C with a flow rate of 30 µl/min. This study presents frequency and dissipation plots corresponding to the 3rd overtone (15 MHz).

The adsorption experiments were started by injecting only PBS buffer in the QCM-D chambers in order to get the baseline, which was followed by the injection of the polymer solutions. Finally, PBS buffer was injected to check the detachment of DCMC-g-PEG and CMC-g-PEG from the collagen IV films.

4. Results and discussion

4.1 Charge of CMC-g-PEG

Direct polyelectrolyte titration was applied to provide evidence of PEG grafting of CMC by the decrease in the polymer charge due to the reduction in carboxyl groups content. Figure 17, 18 and 19 show the change of conductivity of dialyzed CMC, CMC-g-PEG (2) and CMC-g-PEG (5), respectively, as a function of the amount of hydrochloric acid added to the solution. Phase 1 is the neutralization of the excess of NaOH initially added. The conductivity of solution decreased when the strong base groups were neutralised with hydrochloric acid. Phase 2 shows the process of neutralisation of carboxyl groups during which the conductivity increased slightly until all the carboxyl groups were neutralised. In phase 3, the accumulation of hydrochloric acid in excess led to a sharp increase in conductivity.

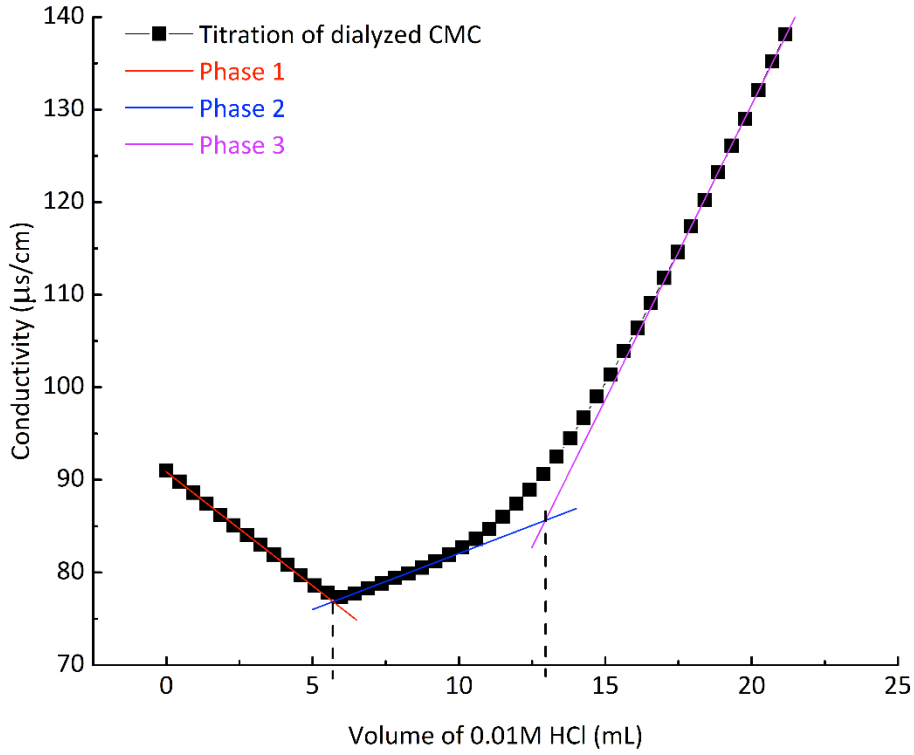

Figure 17. Determination of the total amount of charge of dialyzed CMC

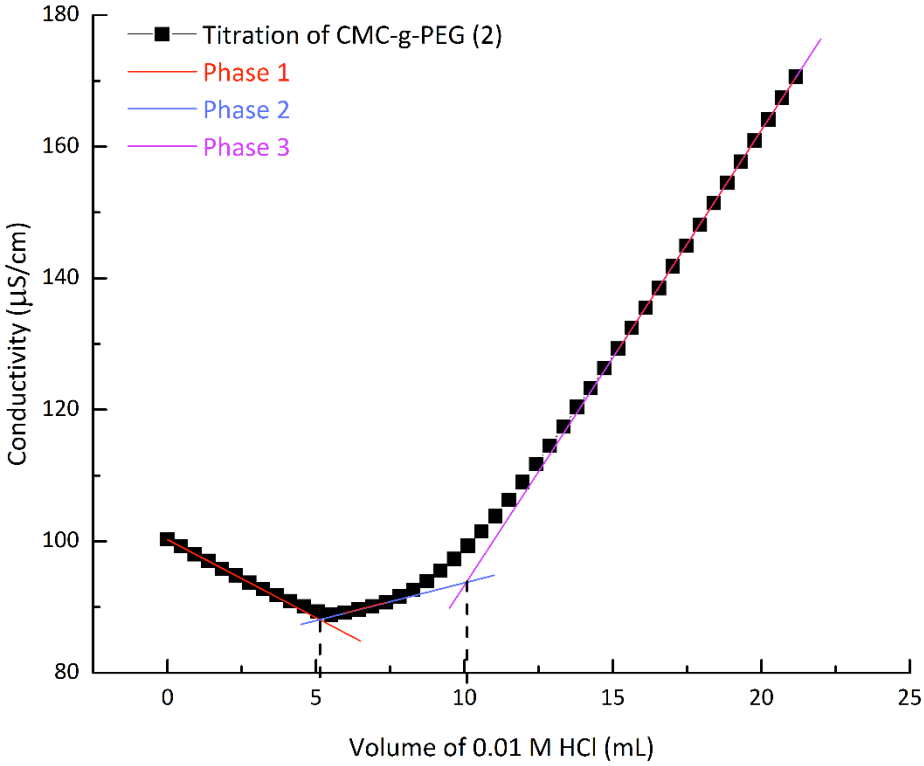

Figure 18. Determination of the total amount of charge of CMC-g-PEG (2)

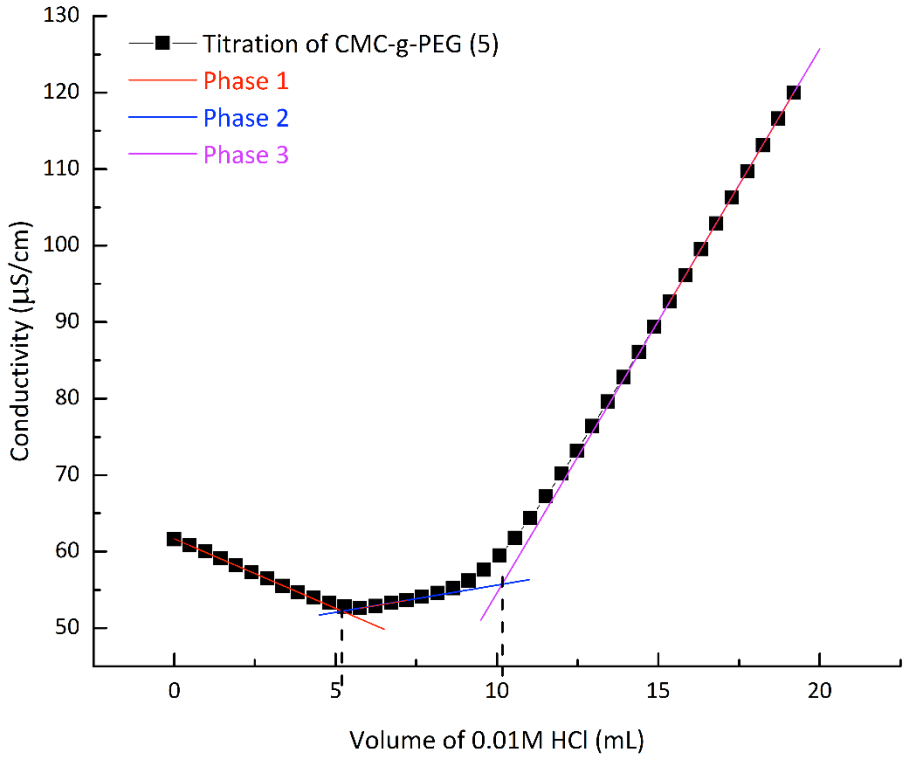

Figure 19. Determination of the total amount of charge of CMC-g-PEG (5)

Polyelectrolyte titration showed a decrease in charge density from 2850±240 µmol/g for dialyzed CMC to 1940±140 µmol/g for CMC-g-PEG (2) and 1950±110 µmol/g for CMC-g-PEG (5). The decrease of charge indicates that almost 5.1 % of the carboxyl groups in CMC have reacted to form CMC-g-PEG (2) and CMC-g-PEG (5), respectively. The carboxyl/amine molar ratio used in the reaction was 1.038 mmol/ 0.126 mmol which means that at least 12.1% of carboxyl groups should be consumed if all OMe-PEG amines were grafted to CMC. However, after calculating the mass values of CMC, OMe-PEG and CMC-g-PEG before and after the reaction, it is estimated that 6.3% of CMC carboxyl groups had been consumed during the preparation of CMC-g-PEG (2) and 3.4% of CMC carboxyl groups had been consumed during the preparation of CMC-g-PEG (5), in good agreement with the results obtained from the conductometric titrations. However, considering that there are more experimental errors in the conductometric titrations, the amount of consumed carboxyl groups calculated from the mass values is more accurate. The yield of CMC-g-PEG (2) in this project is lower than the value in Olszewska *et al*. 2013, where the yield of CMC-g-PEG (2) is about 12.5 %. The possible reason may be the difference of raw material which is CMC and OMe-PEG. In Olszewska's

experiment, the charge of dialyzed CMC is 3600 µmol/g, but the value in this project is around 2850 µmol/g.

The percentage of reduction in carboxyl groups in CMC-g-PEG (2) and CMC-g-PEG (5) indicates the brush density, which is also responsible for the lubricating ability of the polymer. There is one CMC unit with PEG side chain in every 16 or 29 CMC units in CMC-g-PEG (2) and CMC-g-PEG (5), respectively, if the PEG chains are distributed homogeneously along the CMC backbone. In Olszewska's experiment, the brush density is 1:8 which means there is one CMC unit with PEG side chain in every 8 CMC units if the PEG chains are distributed homogeneously (Olszewska et al. 2013a). In Samaroo's experiment, by changing the feed ratio of the side chain (PEG) and the backbone (PAA), the PAA-g-PEGs were synthesized with different brush density. This method to control the brush density may be applied in the further experiments to increase the yield of CMC-g-PEG (Samaroo *et al*. 2017). The effect of the PEG length and graft density for CMC-g-PEG (2) and CMC-g-PEG (5) on properties like lubrication can be studied in future experiments.

4.2 FTIR of CMC-g-PEG

The modification of CMC by grafting PEG chains was confirmed by FTIR spectroscopy. The FTIR spectra of dialyzed CMC is shown in Figure 20, in which it is evident that it shows a broad absorption band at 3440.13 cm^{-1} because of the stretching frequency of the -OH group. The band at 2920.79 cm^{-1} is due to the C-H stretching. The presence of a strong absorption band at 1605.08 cm^{-1} confirms the presence of C=O in carboxyl group (Biswal and Singh 2004). The bands around 1419.11 cm^{-1}, 1384.24 cm^{-1} and 1324.86 cm^{-1} are assigned to C-H bending and -OH bending vibration, respectively. The band at 1263 cm^{-1} indicates the presence of C-O-C stretching in the side chain of CMC, and band at 1060.88 cm^{-1} indicates the presence of >CH-O-CH2 in the CMC backbone (Biswal and Singh 2004).

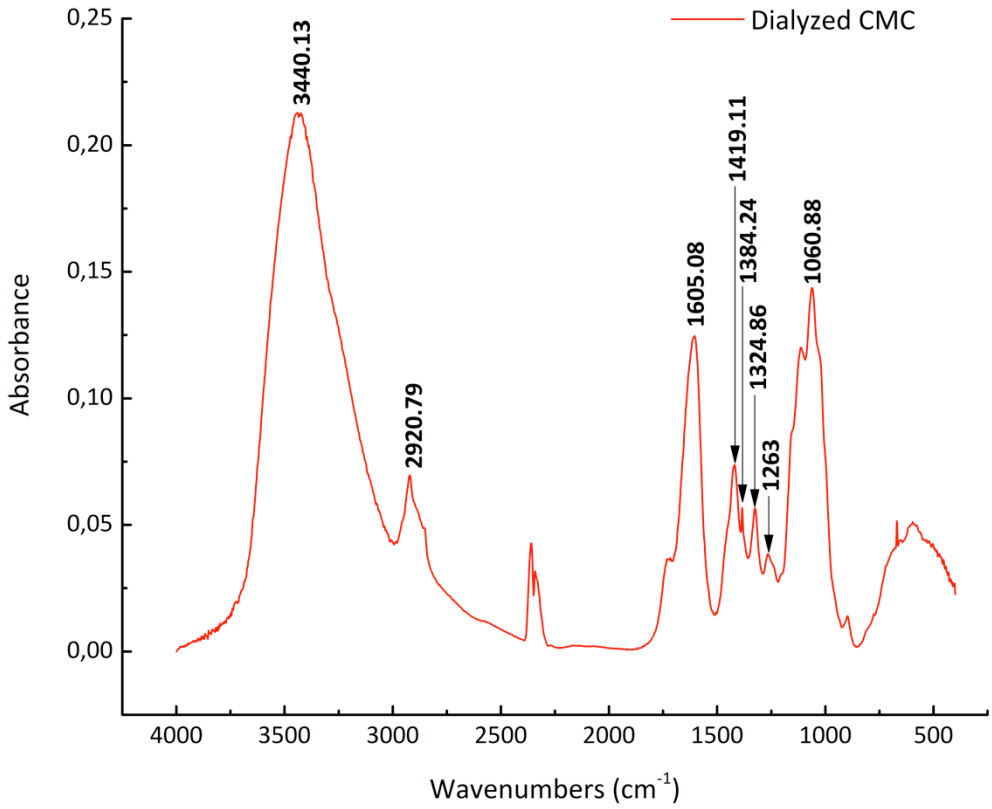

Figure 20. FTIR spectrum of dialyzed CMC.

Figure 21 shows the FTIR spectra of CMC-g-PEG (2) and CMC-g-PEG (5). The band around 3420cm^{-1} indicates the -OH stretching. The band at 2886 cm^{-1} is due to the stretching of C-H bonds of CMC as well as of PEG side chain and the -OH stretching. Compared with the FTIR spectra of dialyzed CMC, the amide bond formation is evidenced by the detection of N-H bending at 1616 cm^{-1} and the C=O stretching at 1683 cm^{-1}. Further, there are strong adsorption of bands at 1109 and 1466 cm^{-1}, which are due to C-O stretching and C-H bending of PEG side chain, respectively.

To compare the absorbance difference between CMC-g-PEG (2) and CMC-g-PEG (5), the spectra is normalized using the band at 3400 cm^{-1} because this band is associated with the -OH groups in the polymer backbone, which is the same in both CMC-g-PEG (2) and CMC-g-PEG (5). The bands at 2886, 1466, 1109 cm^{-1} correspond to C-H stretching, C-H bending and C-O stretching, respectively, and the absorbance at these bands is higher for CMC-g-PEG (5) than for the CMC-g-PEG (2). The only reason why the absorbance at these bands is different

is due to that the molecular weight of OMe-PEG amines used to synthesize CMC-g-PEG (5) was higher than the one used to synthesize CMC-g-PEG (2) (5 kDa and 2 kDa, respectively).

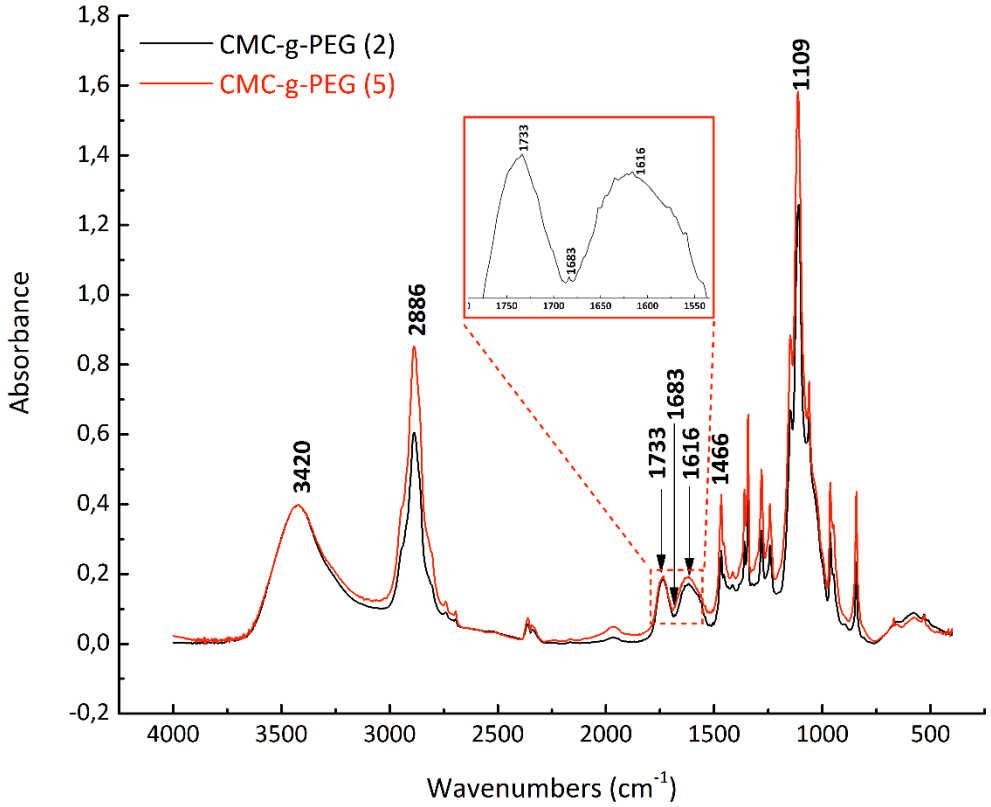

Figure 21. FTIR spectra of CMC-g-PEG (2) and CMC-g-PEG (5)

The FTIR band information of CMC-g-PEG (2) is also compared with the FTIR spectra in Olszewska *et al*. 2013a, where they found the band at 1650 cm^{-1} that could confirm the presence of amide bonds between PEG and CMC. Due to the similar FTIR band information of amide bonds, we ensure that the synthesis of CMC-g-PEG was successful.

Figure 22 shows the difference of absorbance between dialyzed CMC and CMC-g-PEG (2). To compare the absorbance difference between dialyzed CMC and CMC-g-PEG (2), the band at about 3400 cm^{-1} is also used for normalization since this band corresponds to the stretching of the -OH groups in the backbone which are not changed during the reaction. The absorbance of the band at around 2886 and 1109 cm^{-1} of dialyzed CMC experience an obvious increase. This is due to the $-CH_2$ and C-O-C bonds in the PEG side chains. A similar conclusion

can be observed from Figure A1 in the appendix when the FTIR spectra of dialyzed CMC is compared with the FTIR spectra of CMC-g-PEG (5).

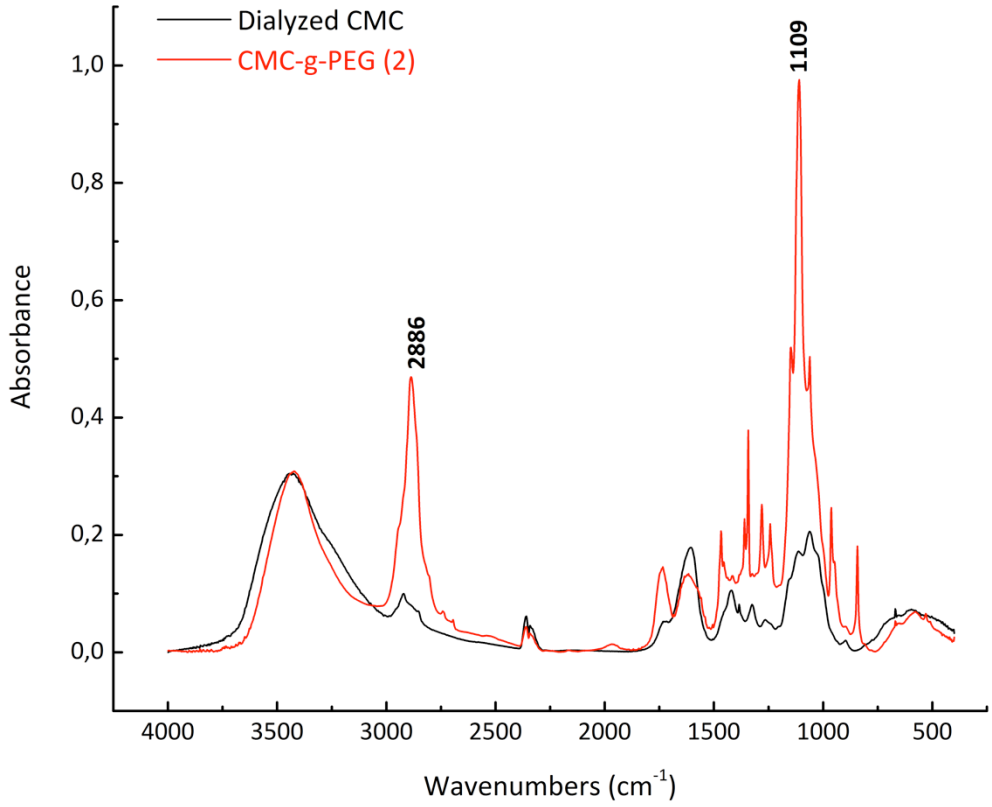

Figure 22. FTIR spectra of dialyzed CMC and CMC-g-PEG (2)

4.3 FTIR of DCMC-g-PEG

The structure of DCMC-g-PEG (2) is confirmed by FTIR spectra shown in Figure 23. It is well known that aldehyde groups exhibit two characteristic FTIR bands at near 1740 and 2800 cm^{-1}, which are due to C=O stretching and C-H stretching, respectively. The band at near 2800 cm^{-1} is also due to the -OH stretching. In the FTIR spectra of DCMC-g-PEG (2), the absorbance of the band at around 1739 cm^{-1} is due to C=O stretching of aldehyde groups. The bands at around 2878 and 2870 cm^{-1} indicate the presence of C-H stretching of aldehyde groups. The band information shown in Figure 23 indicates that the CMC-g-PEG had been selectively oxidized by sodium periodate. The FTIR band information of DCMC-g-PEG is also compared with the FTIR spectra in Li *et al*. 2011, where they found the band at 1738 cm^{-1} that could

confirm the presence of aldehyde groups. Due to the similar FTIR band information of aldehyde groups, we ensure that the synthesis of DCMC-g-PEG was successful.

The FTIR spectra comparison of DCMC-g-PEG (2) and DCMC-g-PEG (5) is also shown in Figure 23 after normalization using the band at about 3400 cm^{-1} again. The main reason why the absorbance bands at 1466 and 1109 cm^{-1} of DCMC-g-PEG (5) is higher than the one of DCMC-g-PEG (2) is because the molecular weight of OMe-PEG amines used to synthesize CMC-g-PEG (5) was higher than the one used to synthesize CMC-g-PEG (2) (5 kDa and 2 kDa, respectively). However, since during the synthesis of DCMC-g-PEG, the molar amount of CMC-g-PEG (2) and CMC-g-PEG (5) were the same, a similar amount of aldehyde groups in DCMC-g-PEG (2) and DCMC-g-PEG (5) is expected. That is confirmed by the similar absorbance observed at bands around 1740 cm^{-1} for DCMC-g-PEG (2) and DCMC-g-PEG (5).

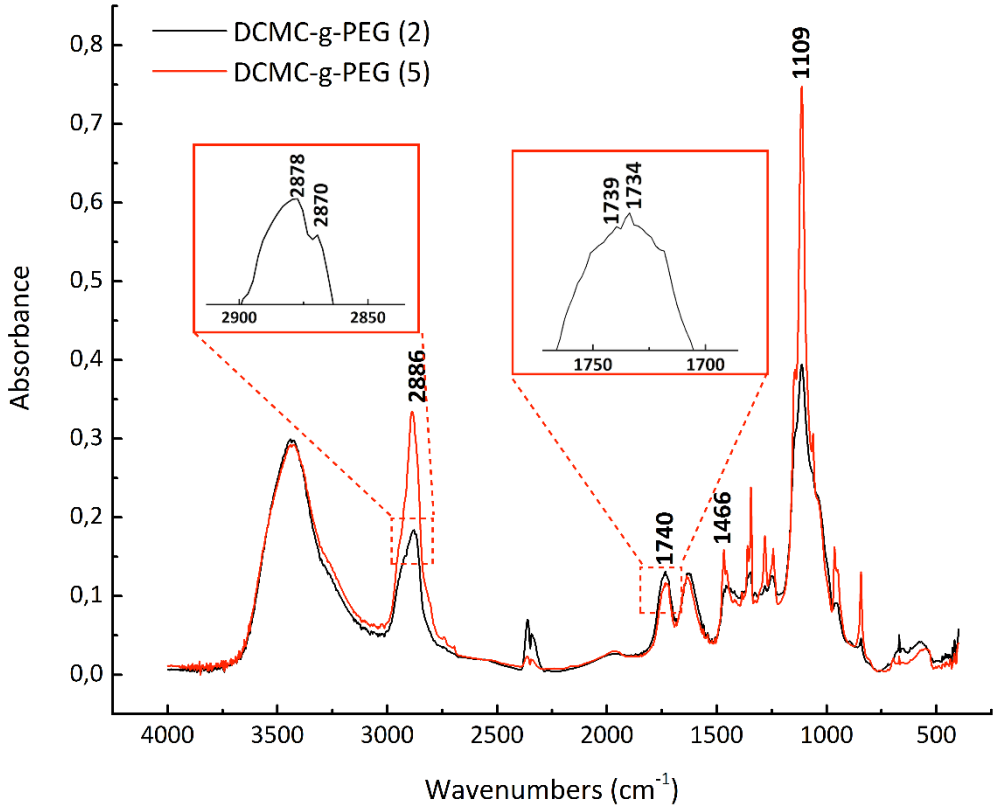

Figure 23. FTIR spectra of DCMC-g-PEG (2) and DCMC-g-PEG (5)

Figure 24 presents the FTIR spectra of CMC-g-PEG (5) and DCMC-g-PEG (5). The FTIR spectra of CMC-g-PEG (5) and DCMC-g-PEG (5) were normalized using the band at around 1109 cm^{-1} since this band corresponds to the stretching of C-O bonds in the PEG side chain, which was not changed during the oxidation of CMC-g-PEG (5) to DCMC-g-PEG (5). Compared with CMC-g-PEG (5), the absorbance of DCMC-g-PEG (5) at band around 2800 cm^{-1} (C-H stretching and -OH stretching) decreases. The reason is that when CMC-g-PEG was oxidized by sodium periodate, -OH groups in the CMC-g-PEG backbone were converted to aldehyde groups. The band at around 1740 cm^{-1} which is responsible for the C=O groups experienced a slight increase due to the synthesis of aldehyde groups. A similar result can also be concluded by the comparison between CMC-g-PEG (2) and DCMC-g-PEG (2) shown in Figure A2 in the appendix.

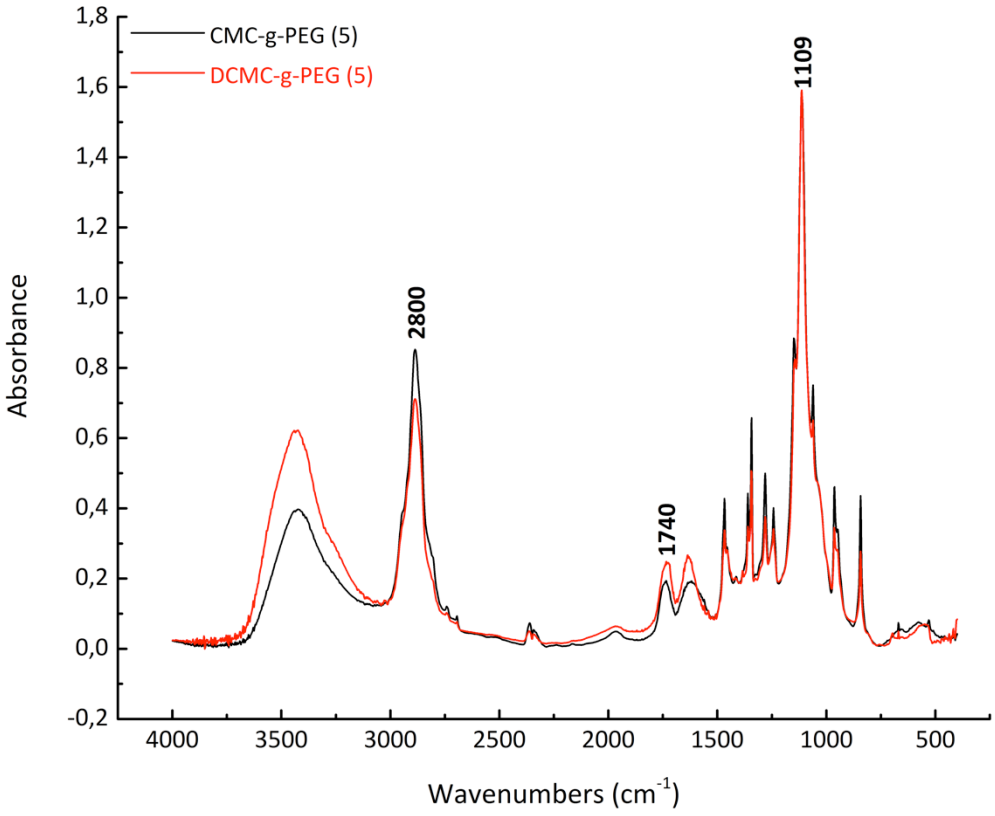

Figure 24. FTIR spectra of CMC-g-PEG (5) and DCMC-g-PEG (5)

4.4 CMC-g-PEG and DCMC-g-PEG adsorption on collagen IV

To better understand the attaching ability of CMC-g-PEG and DCMC-g-PEG to collagen, several adsorption experiments were performed (QCM-D). Prior to the experiment, PBS buffer was injected into the QCM-D chambers in order to obtain a stable baseline.

Figure A3 (a) and A3 (b) in the appendix shows the adsorption curves of dialyzed CMC, CMC-g-PEG (2) and DCMC-g-PEG (2) at the concentration of 100 μg/ml. The *ΔF* started to decrease and the *ΔD* started to increase when the QCM-D sensors were rinsed with polymer solutions. The decrease of *ΔF* indicates the attachment of polymers to the collagen, and lower value of *ΔF* means more polymers that were attached onto the surface of the collagen IV. Meanwhile, the increase of *ΔD* is related to the conformation of the attached polymers. A higher value of dissipation means the attached polymers are in an extended conformation, and the lower value means the polymers are adsorbed in a flatter conformation. Unfortunately, since there were some bubbles in the tube which was used in the CMC-g-PEG (2) experiment, no complete attachment information was obtained for CMC-g-PEG (2). Also, the concentration of polymers was too low to result in a reasonable conclusion.

To generate a more obvious trend of the attachment of polymers to collagen IV, a higher concentration (1 mg/ml) of polymer solutions was employed in the following adsorption experiments. PBS was previously injected to get a good baseline before the experiment. The corresponding frequency and dissipation curves are shown in Figure 25. In the first 5 minutes, the QCM-D gold sensors which had been coated with the collagen IV were rinsed with remained PBS buffer, and then the QCM-D sensors were rinsed with the polymers for almost 95 minutes. Significant changes in frequency are observed for all the polymers, which means that all the types of polymers adsorb on collagen. However, here is a remarkable difference in frequency. For the dialyzed CMC, the frequency drops more obviously than the frequency shown in Figure A3 (a), which means some dialyzed CMC are attached onto the surface of collagen IV. Similarly, because the value of frequency for the CMC-g-PEG (2) shows a decreasing trend, it is reasonable to conclude that some CMC-g-PEG (2) are also attached onto the surface of collagen IV. However, compared with the other two types of polymers, the value of *ΔF* for DCMC-g-PEG (2) experiences a sharp decrease, especially in the first 35 minutes, which indicates that a lot of DCMC-g-PEG (2) have been rapidly attached onto the

surface of collagen IV in this period. More polymers are then attached to the collagen IV in the next 60 minutes with a relatively low rate. After rinsing the QCM-D gold sensors with polymer solutions for 95 minutes, PBS buffer was injected in all the three chambers for another 40 minutes to find out if the adsorbed polymers detached from the collagen films. For both dialyzed CMC and CMC-g-PEG (2), no obvious increase of the value of *ΔF* is observed, which indicates that no polymers detached from collagen IV. However, it also means that there are not many polymers attached onto the surface of collagen IV. The value of *ΔF* for DCMC-g-PEG (2) goes up a little, hence some polymers may detach from the surface of collagen IV in the first 20 minutes. Since the *ΔF* does not increase so much and the value becomes stable in the last 20 minutes, most of attached polymers remains adsorbed onto the surface of collagen IV film. Compared with the results of adsorption experiment in Olszewska et al. 2013a, although the experimental environment is different. For example, the employed substrate is cellulose nanofibrils and the mediums used in the QCM-D experiment are NaAc/HAc for pH4.5 and monopotassium phosphate/Monosodium phosphate (KH2PO4/NaH2PO4) for pH 7.3, similar adsorption result can be observed which is that the attaching ability of dialyzed CMC and CMC-g-PEG is similar based on the similar values of ΔF for CMC and CMC-g-PEG.

The value of *ΔD* for DCMC-g-PEG (2) is much higher than the value for dialyzed CMC and CMC-g-PEG (2) due to a large number of polymers attached onto the surface of collagen IV. In the first 40 minutes, the sharper increase of dissipation compared with the increasing rate in the later 60 minutes for DCMC-g-PEG (2) indicates a high rate of attachment. The same conclusion has been proved by the information provided in Figure 25 (a) and Figure 25 (b). In the last 40 minutes, due to the injection of PBS buffer, the value of *ΔD* for DCMC-g-PEG (2) goes down, and the trend is kept until the end of the experiment. The decreasing value of dissipation for DCMC-g-PEG (2) is due to the detachment of a small fraction of adsorbed polymer, as the frequency curves show. Compared with the dissipation for dialyzed CMC, the value of *ΔD* for CMC-g-PEG (2) is higher because more polymers are attached. When the QCM-D gold sensors were rinsed with PBS buffer, the values of *ΔD* for both dialyzed CMC and CMC-g-PEG (2) drop rapidly, and then remain stable.

A comparison of *ΔD* as a function of *ΔF* for CMC, CMC-g-PEG (2) and DCMC-g-PEG (2) is shown in Figure 25 (c). The slopes of the curves for CMC-g-PEG (2) and DCMC-g-PEG (2) are quite

similar which means the conformation of attached polymer are similar. The only difference of CMC-g-PEG (2) and DCMC-g-PEG (2) is that there are aldehyde groups in the backbone of DCMC-g-PEG (2), and that is the most important reason why there is much more DCMC-g-PEG (2) attached onto the surface of collagen IV compared with CMC-g-PEG (2).

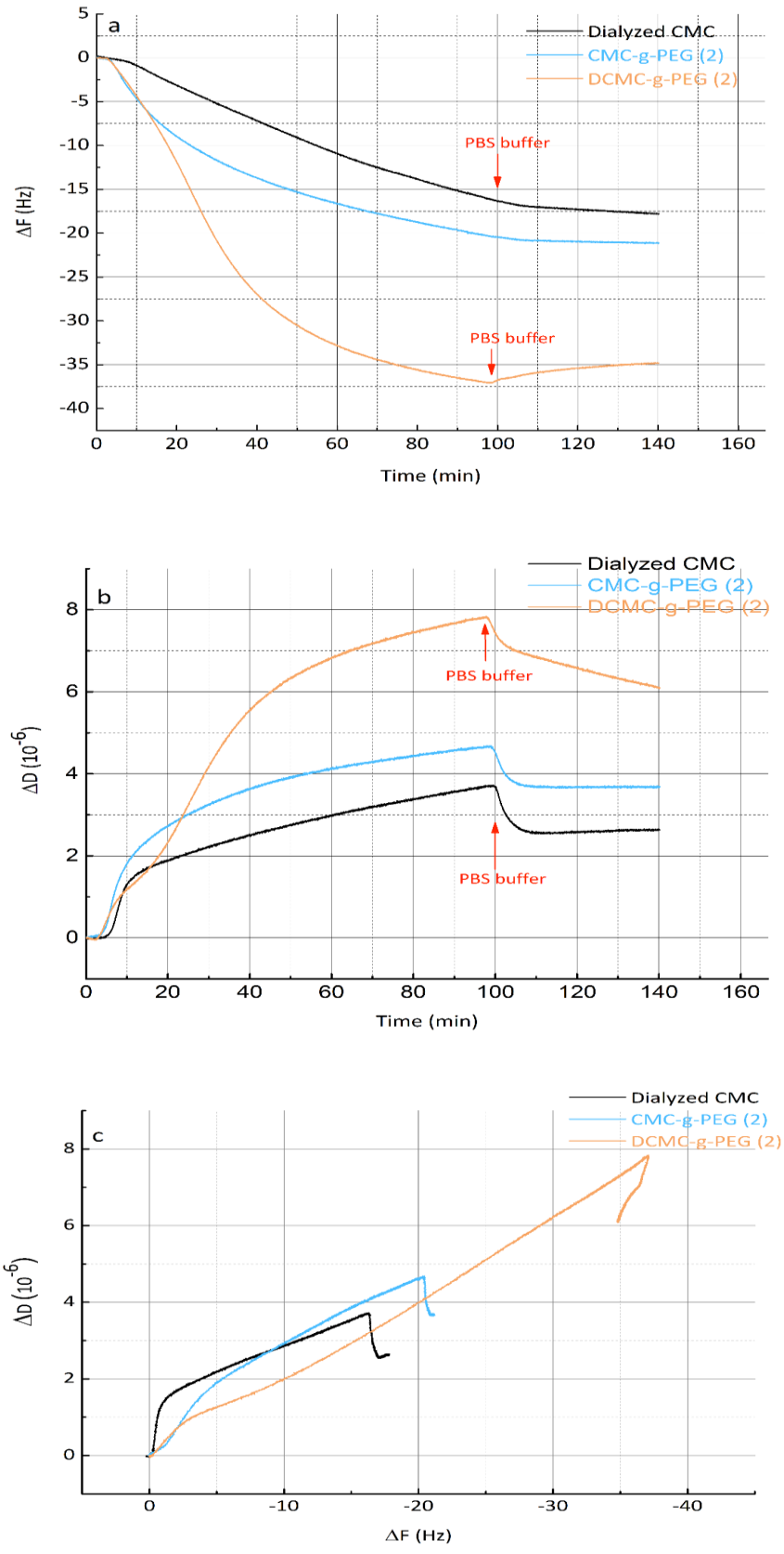

Figure 25. Frequency curves **(a)**, dissipation curves **(b)** and ΔD as a function of ΔF **(c)** for the adsorption of dialyzed CMC, CMC-g-PEG (2) and DCMC-g-PEG (2) onto collagen IV films. The polymer concentration was 1 mg/ml.

Figure 26 shows the adsorption curves of CMC-g-PEG (2), CMC-g-PEG (5), DCMC-g-PEG (2) and DCMC-g-PEG (5) to the collagen IV at the concentration of 1 mg/ml. After obtaining a stable baseline in PBS, the polymer solutions were injected into the QCM-D chambers for 110 minutes. For the CMC-g-PEG (2), the frequency drops rapidly in the first 5 minutes of rinsing with polymer solutions and then keeps a slowing decrease in the following 100 minutes. The similar tendency happens to the curve of CMC-g-PEG (5), the difference is that the final ΔF of CMC-g-PEG (2) is slightly higher in absolute value than the value for CMC-g-PEG (5). By contrast, there is a considerable drop of frequency for the DCMC-g-PEG (2). In the first 40 minutes, the frequency of DCMC-g-PEG (2) experiences a sharp decrease, then followed by a relatively smooth drop in the next 70 minutes. Compared with CMC-g-PEG (2), the value of ΔF for DCMC-g-PEG (2) is much higher in absolute value. The same phenomena are also shown in Figure 25, which indicates that the observed trends were reproducible. However, the decreased value of ΔF for DCMC-g-PEG (2) in Figure 25 is around 37 Hz, but the number for DCMC-g-PEG (2) in Figure 26 is about 27 Hz. For the DCMC-g-PEG (5), similar to the trend of DCMC-g-PEG (2), the value of frequency also drops remarkably in the first 40 minutes and then decreases slowly. However, the value of ΔF for DCMC-g-PEG (5) is much higher in absolute value than the value for CMC-g-PEG (5), even much higher than the value for DCMC-g-PEG (2). Like in other QCM-D experiments, PBS buffer was used to find out the detachment of polymers in the last 30 minutes. No detachment of CMC-g-PEG (2) and CMC-g-PEG (5) was observed, the frequency of CMC-g-PEG (2) and CMC-g-PEG (5) does not show an obvious increase. However, the values for DCMC-g-PEG (2) and DCMC-g-PEG (5) goes up which means a small number of polymers detached from the surface of collagen IV. Figure 26 (a) indicates that the attached mass of DCMC-g-PEG (5) is much higher than the attached mass of DCMC-g-PEG (2). The possible reason is the length of PEG side chain, which is longer for DCMC-g-PEG (5) than for DCMC-g-PEG (2). Although a tiny bubble seems to have entered the chamber and disturb a little the adsorption of DCMC-g-PEG (2) at about 25 min, the effect on the final value of ΔF is probably small since the slope of DCMC-g-PEG (2) is already higher than the slope of DCMC-g-PEG (5) even before the interruption, which means the final frequency of DCMC-g-PEG (2) will still lower than the frequency of DCMC-g-PEG (5) if there is no bubble in the tube. Based on this experiment, it cannot be concluded that the attaching ability of DCMC-g-PEG (5) is better than that of DCMC-g-PEG (2).

The curve of dissipation is used to analyze the conformation of attached polymers. For CMC-g-PEG (2) and CMC-g-PEG (5), the dissipations increased rapidly in the first 10 minutes, and then the values kept increasing smoothly. When the PBS buffer was employed to rinse the gold sensors, the values experienced a fast drop and then keep stable. For the DCMC-g-PEG (2) and DCMC-g-PEG (5), the changes in ΔD correlate with the changes in ΔF showed in Figure 26 (a). In the first 40 minutes, the values of dissipation increased dramatically, followed by a slow increase in the next 70 minutes. Due to the higher adsorption of DCMC-g-PEG polymers, the values of dissipation for DCMC-g-PEG (2) and DCMC-g-PEG (5) are much higher than the values for CMC-g-PEG (2) and CMC-g-PEG (5). The high values of dissipation also correlate with the conformations of the attached polymers. According to the information provided in Figure 26 (c), the value of slope of ΔD *versus* ΔF curves for DCMC-g-PEG (2) is slightly higher than the value for DCMC-g-PEG (5), which seems to indicate that the conformation of attached DCMC-g-PEG (5) is a bit more compact than the attached DCMC-g-PEG (2). By comparison between CMC-g-PEG (5) and DCMC-g-PEG (5), the conformation of attached polymer is quite similar and the only difference is the amount of attached polymer. It is obvious that there is much more DCMC-g-PEG (5) attached onto the surface of collagen IV than CMC-g-PEG (5). The only reason is that there are aldehyde groups in the backbone of DCMC-g-PEG (5).

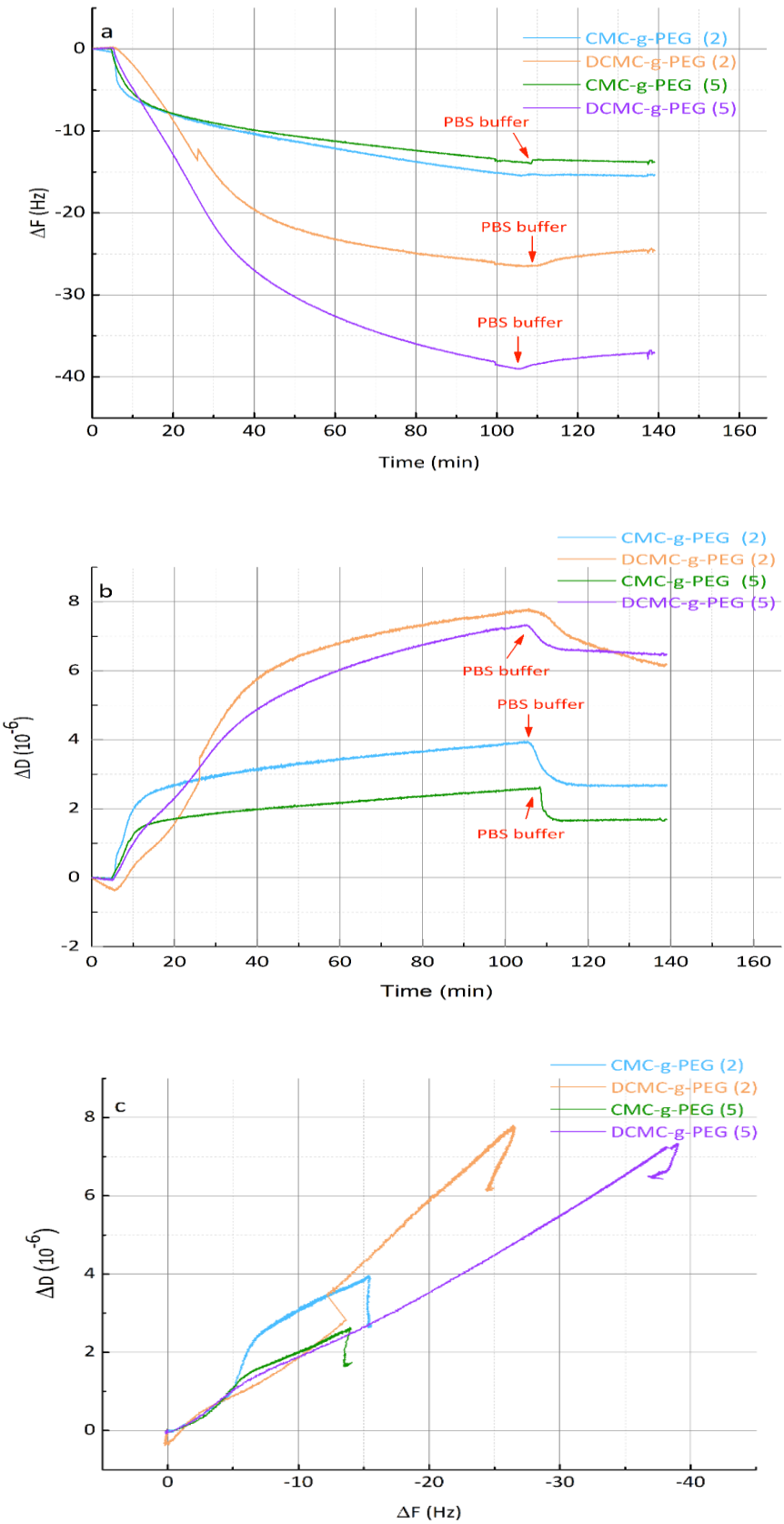

Figure 26. Frequency curves **(a)**, dissipation curves **(b)** and ΔD as a function of ΔF **(c)** for the adsorption of CMC-g-PEG (2), DCMC-g-PEG (2), CMC-g-PEG (5) and DCMC-g-PEG (5) onto collagen IV films. The polymer concentration was 1 mg/ml.

Based on the adsorption results of dialyzed CMC, CMC-g-PEG and DCMC-g-PEG, the aldehyde group is the most significant reason why the attaching ability of DCMC-g-PEG to the collagen IV is much better than any other polymers. Further, the conformation of the attached DCMC-g-PEGs is mainly affected by the length of side chains: longer side chains cause more compact conformation. However, due to the small number of attached CMC-g-PEG (2) and CMC-g-PEG (5) on the collagen IV, the attached CMC-g-PEG (2) and CMC-g-PEG (5) show similar conformation.

5. Conclusions

CMC-g-PEG is a promising brush-like polymer which could be used for the treatment of damaged cartilage. The properties of CMC including biocompatibility, high viscosity, transparency, hydrophilicity, non-toxicity, moisture sorption property, biodegradability, and lubrication are considered as highly beneficial in biomedical applications. In this master thesis work, CMC-g-PEGs with different PEG lengths (2 kDa and 5 kDa) were synthesized and characterized by conductometric titration and FTIR. The reduction in the number of carboxyl groups in conductometric titration experiment and the presence of amide bonds in the FTIR spectra of CMC-g-PEG indicated that the PEG side chain had been successfully attached to CMC. The adsorption of CMC-g-PEGs on collagen IV (first approach model for cartilage) was then studied by QCM-D. However, although it has been proved before that CMC-g-PEG has very good lubrication properties, the attaching ability of CMC-g-PEG to cartilage has not been extensively investigated. Since the good attachment of polymers to the cartilage is crucial in the potential applications of the polymer in cartilage treatments (the polymers have to be always connected with the surface of the cartilage to ensure they can show the remarkable lubricating ability), aldehyde groups were introduced in CMC-g-PEG by $NaIO_4$ oxidation to get DCMC-g-PEG in order to improve the attachment to collagen. DCMC-g-PEG was synthesized and characterized by FTIR. Absorbance bands at 1739.08, 2878.18 and 2870.06 cm^{-1} associated to C=O and C-H stretching of aldehyde groups, respectively, were observed in the FTIR spectra of DCMC-g-PEG.

The attaching ability of CMC-g-PEG and DCMC-g-PEG with different lengths of PEG side chain to collagen was studied. QCM-D results show that, although dialyzed CMC and CMC-g-PEG

can absorb onto the surface of collagen IV, the adsorbed amount is clearly less than with DCMC-g-PEG. Some CMC-g-PEG can be absorbed on collagen IV, and the attached amount of CMC-g-PEG (2) to the collagen IV is similar to the amount of CMC-g-PEG (5), no matter the size of the PEG side chain. By contrast, a high amount of DCMC-g-PEG (2) and DCMC-g-PEG (5) can be attached onto the surface of collagen IV, enhanced by the covalent bonds between aldehyde groups of DCMC-g-PEG and amine groups of collagens. Therefore, it can be concluded that the introduction of aldehyde groups to the backbone of CMC-g-PEG is the key process to increase the attaching ability of CMC-g-PEG.

However, due to the limitation of time, there are some experiments needed to be finished in the future work. To try to increase the yield of CMC-g-PEG and DCMC-g-PEG, to investigate the difference in lubrication between the polymers with different PEG chains, and to test the biocompatibility and the adsorption of the polymers on real cartilage are some experiments that need to be accomplished in the future.

References

ATESHIAN, G.A., 2009. The role of interstitial fluid pressurization in articular cartilage lubrication. Journal of Biomechanics, 42, pp. 1163-1176.

BAKER, M.I., WALSH, S.P., SCHWARTZ, Z. and BOYAN, B.D., 2012. A review of polyvinyl alcohol and its uses in cartilage and orthopedic applications. Journal of biomedical Materials research B: Applied Biomaterials, 100B(5), pp. 1451-1457.

BALASUNDARAM, G., STOREY, D.M. and WEBSTER, T.J., 2014. Novel nano-rough polymers for cartilage tissue engineering. International Journal of Nanomedicine, 9, pp. 1845-1853.

BAUER, C., BERGER, M., BAUMGARTNER, M.B., HÖLLER, S., ZWICKL, H., NICULESCU-MORZSA, E., HALBWIRTH, F. and NEHRER, S., 2016. A Novel Cross-Linked Hyaluronic Acid Porous Scaffold for Cartilage Repair: An In Vitro Study with Osteoarthritic Chondrocytes. Cartilage, 7(3), pp. 265-273.

BENZ, M., CHEN, N.H. and ISRAELACHVILI, J., 2004. Lubrication and wear properties of grafted polyelectrolytes, hyaluronan and hylan, measured in the surface forces apparatus. Journal of

Biomedical Materials Research, Part A, 71(1), pp. 6-15.

BISWAL, D.R. and SINGH, R.P., 2004. Characterisation of carboxymethyl cellulose and polyacrylamide graft copolymer. Carbohydrate Polymers, 57(4), pp. 379-387.

BUCKWALTER, J.A. and MANKIN, H.J., 1998. Articular cartilage: degeneration and osteoarthritis, repair, regeneration, and transplantation. Instructional Course Lectures, 47, pp. 487-504.

BUCKWALTER, J.A. and Martin, J.A., 2006. Osteoarthritis. Advanced Drug Delivery Reviews, 58, pp. 150-167.

BUSIJA, L., BRIDGETT, L., WILLIAMS, S.R.M., OSBORNE, R.H., BUCHBINDER, R., MARCH, L. and FRANSEN, M., 2010. Osteoarthritis. Best Practice & Research Clinical Rheumatology, 24, pp. 757-768.

CHANG, C., DUAN, B., CAI, J. and ZHANG, L., 2010. Superabsorbent hydrogels based on cellulose for smart swelling and controllable delivery. European Polymer Journal, 46, pp. 92-100.

CHANG, C., ZHANG, L., 2011. Cellulose-based hydrogels: Present status and application prospects. Carbohydrate Polymers, 84, pp. 40-53.

CHAWLA, K., LEE, S., LEE, B.P., DALSIN, J.L., MESSERSMITH, P.B. and SPENCER, N.D., 2009. A novel low-friction surface for biomedical applications: modification of poly(dimethylsiloxane) (PDMS) with polyethylene glycol (PEG)-dopa-lysine. Journal of Biomedical Materials Research Part A, 90(3), pp. 742-749.

CZANDEMA, A.W., LU, C., 1984. Applications of piezoelectric quartz crystal microbalances. Amsterdam: Elsevier Science Publishers.

DIXON, M.C., 2008. Quartz Crystal Microbalance with Dissipation Monitoring: Enabling Real-Time Characterization of Biological Materials and Their Interactions. Journal of Biomolecular Techniques, 19(3), pp. 151-158.

DOULABI, A.H., MEQUANINT, K. and MOHAMMADI, H., 2014. Blends and Nanocomposite Biomaterials for Articular Cartilage Tissue Engineering. Materials, 7, pp. 5327-5355.

DROBEK, T., SPENCER, N.S., 2008. Nanotribology of Surface-Grafted PEG Layers in an Aqueous Environment. Langmuir, 24, pp. 1484-1488.

ECKSTEIN, F., TIESCHKY, M., FABER, S., ENGLMEIER, K. and REISER, M., 1999. Functional analysis of articular cartilage deformation, recovery, and fluid flow following dynamic exercise in vivo. Anat Embryol, 200, pp. 419-424.

EI-SAKHAWY, M., KAMEL, S., SALAMA, A. and SARHAN, H.A., 2014. Carboxymethyl Cellulose Acetate Butyrate: A Review of the Preparations, Properties, and Applications. Journal of Drug Delivery, 2014, pp. 1-6.

ERONEN, P., JUNKA, K., LAINE, J. and ÖSTERBERG, M., 2011. Interaction Between Water-Soluble Polysaccharides and Native Nanofibrillar Cellulose Thin Films. BioResources, 6(4), PP. 4200-4217.

FELSON D.T., LAWRENCE R.C., DIEPPE P.A., HIRSCH R., HELMICK CG, JORDAN J.M. *et al*., 2000. Osteoarthritis: New Insights. Part 1: The Disease and Its Risk Factors. Annals of Internal Medicine, 133, pp. 635-646.

FERREIRA, G.N.M., DA-SILVA, A.C. and TOME, B., 2009. Acoustic wave biosensors: physical models and biological applications of quartz crystal microbalance. Trends in Biotechnology, 27(12), pp. 689-697.

FOX, A.J.S., BEDI, A. and RODEO, S.A., 2009. The Basic Science of Articular Cartilage: Structure, Composition, and Function. Sports Health, 1(6), pp. 461-468.

GAIHRE, B., JAYASURIYA, A.C., 2016. Fabrication and characterization of carboxymethyl cellulose novel microparticles for bone tissue engineering. Materials Science and Engineering C, 69, pp. 733-743.

GALE, L.R., CHEN, Y. HILLS, B.A. and CRAWFORD, R., 2007. Boundary lubrication of joints: Characterization of surface-active phospholipids found on retrieved implants. Acta Orthopaedica, 78(3), pp. 309-314.

GREENE, G.W., OLSZEWSKA, A., ÖSTERBERG, M., ZHU, H. and HORN, R., 2014. A cartilage-inspired lubrication system. Soft Matter, 10, pp. 374-382.

GUPTA, S., HAWKER, G.A., LAPORTE, A., CROXFORD, R. and COYTE, P.C., 2005. The economic burden of disabling hip and knee osteoarthritis (OA) from the perspective of individuals living with this condition. Rheumatology, 44, pp. 1531-1537.

HABIBI, N., 2014. Preparation of biocompatible magnetite-carboxymethyl cellulose nanocomposite: Characterization of nanocomposite by FTIR, XRD, FESEM and TEM. Spectrochimica Acta Part A: Molecular and Biomolecular Spectroscopy, 131, pp. 55-58.

HEINZE, T., PFEIFFER, K., 1999. Studies on the synthesis and characterization of carboxymethylcellulose. Die Angewandte Makromolekulare Chemie, 266, pp. 37-45.

HILLS, B.A., 2002. Surface-active phospholipid: a Pandora's box of clinical applications. Part II. Barrier and lubricating properties. Internal Medicine Journal, 32, pp. 242-251.

HILLS, B.A., CRAWFORD, R.W., 2003. Normal and Prosthetic Synovial Joints Are Lubricated by Surface-Active Phospholipid: A Hypothesis. The Journal of Arthroplasty, 18(4), pp. 499-505.

HORTON, W.A., HALL, J.G. and HECHT, J.T., 2007. Achondroplasia. The Lancet, 370, pp. 162-172.

HUA, Y., LIUA, L., GUC, Z., DANA, W., DANA, N. and YU, X., 2014. Modification of collagen with a natural derived cross-linker, alginate dialdehyde. Carbohydrate Polymers, 102, pp. 324-332.

HUNTER, D.J., 2011. Osteoarthritis. Best Practice & Research Clinical Rheumatology, 25, pp. 801-814.

JAHN, S., SEROR, J. and KLEIN, J., 2016. Lubrication of Articular Cartilage. Annual. Review of Biomedical Engineering, 18, pp. 235-258.

JIANG, L., LI, Y., WANG, X., ZHANG, L., WEN, J. and GONG, M., 2008. Preparation and properties of nano-hydroxyapatite/chitosan/carboxymethyl cellulose composite scaffold. Carbohydrate Polymers, 74, pp. 680-684.

JOHANNSMANN, D., MATHAUER, K., WEGNER, G. and KNOLL, W, 1992. Viscoelastic properties of thin films probed with a quartz-crystal resonator. Physical Review B, 46(12), pp, 7808-7815.

JONES, A.R.C., GLEGHORN, J.P., HUGHERS, C.E., FITZ, L.J., ZOLLNER, R., WAINWRIGHT, S.D., CATERSON, B., MORRIS, E.A., BONASSAR, L.J. and FLANNERY, C.R., 2007. Binding and Localization of Recombinant Lubricin to Articular Cartilage Surfaces. Journal of Orthopaedic Research, 25(3), pp. 283-292.

KIM, B.S., PARK, I.K., HOSHIBA, T., JIANG, H.L., CHOI, Y.J., AKAIKE, T. and CHO, C.S., 2011. Design of artificial extracellular matrices for tissue engineering. Progress in Polymer Science, 36, pp. 238-268.

KITANO, K., INOUE, Y., MATSUNO, R., TAKAI, M. and ISHIHARA, K., 2009. Nanoscale evaluation of lubricity on well-defined polymer brush surfaces using QCM-D and AFM. Colloids and Surfaces B: Biointerfaces, 74, pp. 350-357.

KONO, H., 2014. Characterization and properties of carboxymethyl cellulose hydrogels crosslinked by polyethylene glycol. Carbohydrate Polymers, 106, pp. 84-93.

KUBO, M., ANDO, K., MIMURA, T., MATSUSUE, Y. and MORI, K., 2009. Chondroitin sulfate for the treatment of hip and knee osteoarthritis: Current status and future trends. Life Sciences, 85, pp. 477-483.

LEE, S., PARK, Y.H. and KI, C.S., 2016. Fabrication of PEG–carboxymethylcellulose hydrogel by thiol-norbornene photo-click chemistry. International Journal of Biological Macromolecules, 83, pp. 1-8.

LEE, S.Y., NAKAGAWA, T. and REDDI, A.H., 2008. Induction of chondrogenesis and expression of superficial zone protein (SZP)/lubricin by mesenchymal progenitors in the infrapatellar fat pad of the knee joint treated with TGF-b1 and BMP-7. Biochemical and Biophysical Research Communications, 376, pp. 148-153.

LI, H., WU, B., MU, C. and LIN, W., 2011. Concomitant degradation in periodate oxidation of carboxymethyl cellulose. Carbohydrate Polymers, 84, pp. 881-886.

LIAO, I.C., MOUTOS, F.T., ESTES, B.T., ZHAO, X.H. and GUILAK, F., 2013. Composite Three-Dimensional Woven Scaffolds with Interpenetrating Network Hydrogels to Create Functional Synthetic Articular Cartilage. Advanced Functional Materials, 23(47), pp. 5833-5839.

LIU, G., ZHANG, G., 2013. SpringerBriefs in Molecular Science, QCM-D Studies on Polymer Behavior at Interfaces. Springer.

LU, X.L., MOW V.C., 2008. Biomechanics of Articular Cartilage and Determination of Material Properties. Medicine and Science in Sports Exercise, 40(2), pp. 193-199.

MA, R., XIONG, D.S., MIAO, F. ZHANG, J. and PENG, Y., 2009. Novel PVP/PVA hydrogels for articular cartilage replacement. Materials Science and Engineering C, 29, pp. 1979-1983.

MANSOUR, J.M., 2003. Biomechanics of cartilage. Kinesiology: the mechanics and pathomechanics of human movement. Wolters Kluwer Health Publishers.

MARX, K.A., 2003. Quartz Crystal Microbalance: A Useful Tool for Studying Thin Polymer Films and Complex Biomolecular Systems at the Solution-Surface Interface. Biomacromolecules, 4(5), pp. 1099-1120.

MCNARY, S.M., ATHANASIOU, K.A. and REDDI, A.H., 2012. Engineering Lubrication in Articular Cartilage. Tissue Engineering: Part B, 18(2), pp. 88-100.

MODIN, C., STRANNE, A., FOSS, M., DUCH, M., JUSTESEN, J., CHEVALLIER, J., ANDERSEN, L.K., HEMMERSAM, A.G., PEDERSEN, F.S. and BESENBACHER, F., 2006. QCM-D studies of attachment and differential spreading of pre-osteoblastic cells on Ta and Cr surfaces. Biomaterials, 27(8), pp. 1346-1354.

MORGESE, G., TRACHSEL, L., ROMIO, M., DIVANDARI, M., RAMAKRISHNA, S.N. and BENETTI, E.M., 2016. Topological Polymer Chemistry Enters Surface Science: Linear versus Cyclic Polymer Brushes. Angewandte Chemie, 55(50), pp. 15583-15588.

MORGESE, G., CAVALLI, E., MÜLLER, M., ZENOBI-WONG, M. and BENETTI, E.M., 2017. Nanoassemblies of Tissue-Reactive, Polyoxazoline Graft-Copolymers Restore the Lubrication Properties of Degraded Cartilage. American Chemical Society, 11, pp. 2794-2804.

MU, C., GUO, J., LI, X. LIN, W. and LI, D., 2012. Preparation and properties of dialdehyde carboxymethyl cellulose crosslinked gelatin edible films. Food Hydrocolloids, 27, pp. 22-29.

NINAN, N., MUTHIAH, M., PARK, I.K., ELAIN, A., THOMAS, S. and GROHENS, Y., 2013.

Pectin/carboxymethyl cellulose/microfibrillated cellulose composite scaffolds for tissue engineering. Carbohydrate Polymers, 98, pp. 877-885.

NISKANEN, R.O., 2005. Early repetitive radiography is unnecessary after an uncomplicated cemented hip or knee arthroplasty for osteoarthritis. Acta Orthopaedica Belgica, 71(6), pp. 692-695.

OGUSHI, Y., SAKAI, A. and KAWAKAMI, K., 2007. Synthesis of Enzymatically-Gellable Carboxymethylcellulose for Biomedical Applications. Journal of Bioscience and Bioengineering, 104(1), pp. 30-33.

OLSZEWSKA, A., JUNKA, K., NORDGREN, N., LAINE, J., RUTLANDBC M.W. and ÖSTERBERG, M., 2013a. Non-ionic assembly of nanofibrillated cellulose and polyethylene glycol grafted carboxymethyl cellulose and the effect of aqueous lubrication in nanocomposite formation. Soft Matter, 9, pp. 7448-7457.

OLSZEWSKA, A., VALLE-DELGADO, J.J., NIKINMAA, M., LAINE, J. and ÖSTERBERG, M., 2013b. Direct measurements of non-ionic attraction and nanoscaled lubrication in biomimetic composites from nanofibrillated cellulose and modified carboxymethylated cellulose. Nanoscale, 2013, 5, pp. 11837-11844.

OUN, A.A., RHIM, J.W, 2015. Preparation and characterization of sodium carboxymethyl cellulose/cotton linter cellulose nanofibril composite films. Carbohydrate Polymers, 127, pp. 101-109.

OZTURK, H.E., STOFFEL, K.K., JONES, C.F. and STACHOWIAK, G.W., 2004. The effect of surface-active phospholipids on the lubrication of osteoarthritic sheep knee joints: Friction. Tribology Letters, 16(4), pp. 283-289.

PARK, H., CHOI, B., HU, C. and LEE, M., 2013. Injectable chitosan hyaluronic acid hydrogels for cartilage tissue engineering. Acta Biomaterialia, 9, pp. 4779-4786.

PEAT, G., MCCARNEY, R. and CROFT, P., 2001. Knee pain and osteoarthritis in older adults: a review of community burden and current use of primary health care. Annals of the Rheumatic Diseases, 60, pp. 91-97.

PELESHANKO, S., TSUKRUK, V.V., 2008. The architectures and surface behavior of highly branched molecules. Progress in Polymer Science, 33, pp. 523-580.

PROULX, A.M. and ZRYD, T.W., 2009. Costochondritis: Diagnosis and Treatment. American Family Physician, 80(6), pp. 617-620.

RODAHL, M., HOOK, F., KROZER, A. and KASEMO, B.H., 1995. Quartz crystal microbalance setup for frequency and Q-factor measurements in gaseous and liquid environments. Review of Scientific Instruments, 66(7), pp. 3924-3930.

SAMAROO, K.J., TAN, M., PUTNAM, D. and BONASSAR, L.J., 2017. Binding and Lubrication of Biomimetic Boundary Lubricants on Articular Cartilage. Journal of Orthopaedic Research, 35(3), pp. 548-557.

SAUERBREY, G., 1959. The use of quartz oscillators for weighing thin layers and for microweighing. Zeitschrift für Physik, 155, pp. 206-222.

SCHMIDT, T.A., GASTELUM, N.S., NGUYEN, Q.T., SCHUMACHER, B.L. and SAH, R.L., 2007. Boundary Lubrication of Articular Cartilage, Role of Synovial Fluid Constituents, 56(3), pp. 882-891.

SEROR, J., MERKHER, Y., KAMPF, N., COLLINSON, L., DAY, A.J., MAROUDAS, A. and KLEIN, J., 2011. Articular Cartilage Proteoglycans As Boundary Lubricants: Structure and Frictional Interaction of Surface-Attached Hyaluronan and Hyaluronan Aggrecan Complexes. Biomacromolecules, 12, pp. 3432-3443.

SHI, Y., XIONG, D.S., 2013. Microstructure and friction properties of PVA/PVP hydrogels for articular cartilage repair as function of polymerization degree and polymer concentration. Wear, 305, pp. 280-285.

SHIOW-FERN, N., NAFISAH, J., 2014. Carboxymethyl cellulose wafers containing antimicrobials: A modern drug delivery system for wound infections. European Journal of Pharmaceutical Sciences, 51, pp. 173-179.

SLAVIN, S., SOERIYADI, A.H., VOORHAAR, L., WHITTAKER, M.R., BECER, C.R., BOYER, C., DAVIS, T.P. and HADDLETON, D.M., 2012. Adsorption behaviour of sulfur containing polymers to gold

surfaces using QCM-D. Soft Matter, 8, pp. 118-128.

SPILLER, K.L., MAHER, S.A. and LOWMAN, A.M., 2011. Hydrogels for the Repair of Articular Cartilage Defects. Tissue Engineering: Part B, 17(4), pp. 281-299.

STAMMEN, J.A., WILLIAMS, S., KU, D.N. and GULDBERG, R.E., 2001. Mechanical properties of a novel PVA hydrogel in shear and unconfined compression. Biomaterials, 22, pp. 799-806.

SUH, J.K.F. and MATTHEW, H.W.T., 2000. Application of chitosan-based polysaccharide biomaterials in cartilage tissue engineering: a review. Biomaterials, 21, pp. 2589-2598.

TEOTIA, A., 2012. Modification of carboxymethyl cellulose through oxidation. Carbohydrate Polymers, 87, pp. 457-460.

UGWOKE, M.I., KAUFMANN, G., VERBEKE, N. and KINGET, R., 2000. Intranasal bioavailability of apomorphine from carboxymethylcellulose-based drug delivery systems. International Journal of Pharmaceutics, 202, pp. 125-131.

VALLE-DELGADO, J.J., JOHANSSON, L.S. and ÖSTERBERG, M., 2016. Bioinspired lubricating films of cellulose nanofibrils and hyaluronic acid. Colloids and Surfaces B: Biointerfaces, 138, pp. 86-93.

VINCENT, T.L. and WATT, F.E., 2010. Osteoarthritis. Medicine, 38, pp. 151-156.

VOINOVA, M.V., JONSON, M. and KASEMO, B., 2002. 'Missing mass' effect in biosensor's QCM applications. Biosensors and Bioelectronics, 17, pp. 835-841.

WANG, X., WANG, Y., LI, L., GU, Z. and YU, X., 2015. Feasibility study of the naturally occurring dialdehyde carboxymethyl cellulose for biological tissue fixation. Carbohydrate Polymers, 115, pp. 54-61.

WATHIER, M. LAKIN, B.A., BANSAL, P.N., STODDART, S.S., SNYDER, B.D. and GRINSTAFF, M.W., 2013. A Large-Molecular-Weight Polyanion, Synthesized via Ring-Opening Metathesis Polymerization, as a Lubricant for Human Articular Cartilage. Journal of the American Chemical Society, 135, pp. 4930-4933.

YADAV, M., RHEE, K.Y., JUNG, I.H. and PARK, S.J., 2013. Eco-friendly synthesis,

characterization and properties of a sodium carboxymethyl cellulose/graphene oxide nanocomposite film. Cellulose, 20, pp. 687-698.

YADOLLAHI, M., NAMAZI, H. and BARKHORDARI, S., 2014. Preparation and properties of carboxymethyl cellulose/layered double hydroxide bionanocomposite films. Carbohydrate Polymers, 108, pp. 83-90.

YU, J., BANQUY, X., GREENE, G.W., LOWREY, D.D. and ISRAELACHVILI, J.N., 2012. The Boundary Lubrication of Chemically Grafted and Cross-Linked Hyaluronic Acid in Phosphate Buffered Saline and Lipid Solutions Measured by the Surface Forces Apparatus. Langmuir, 28, pp. 2244-2250.

Appendix

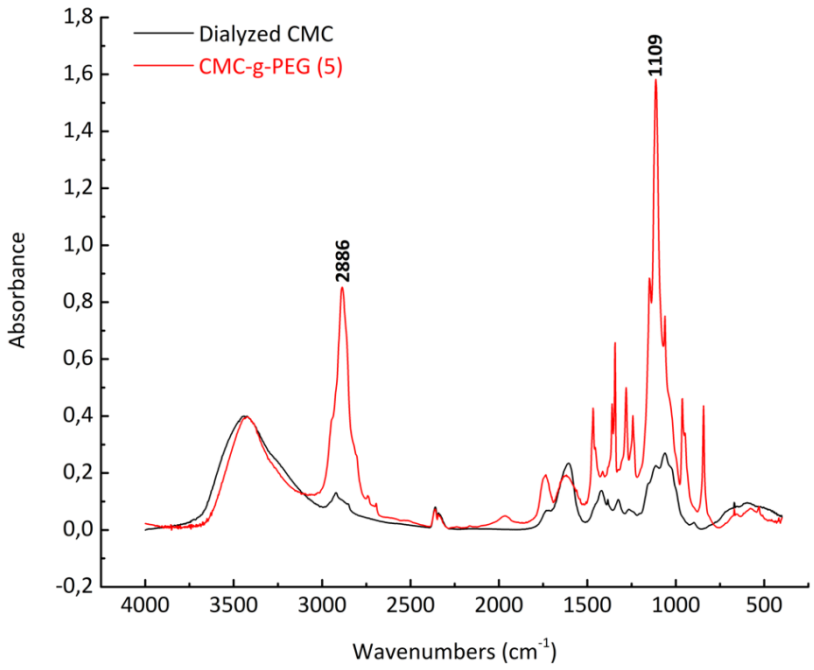

Figure A1. FTIR spectra of dialyzed CMC and CMC-g-PEG (5).

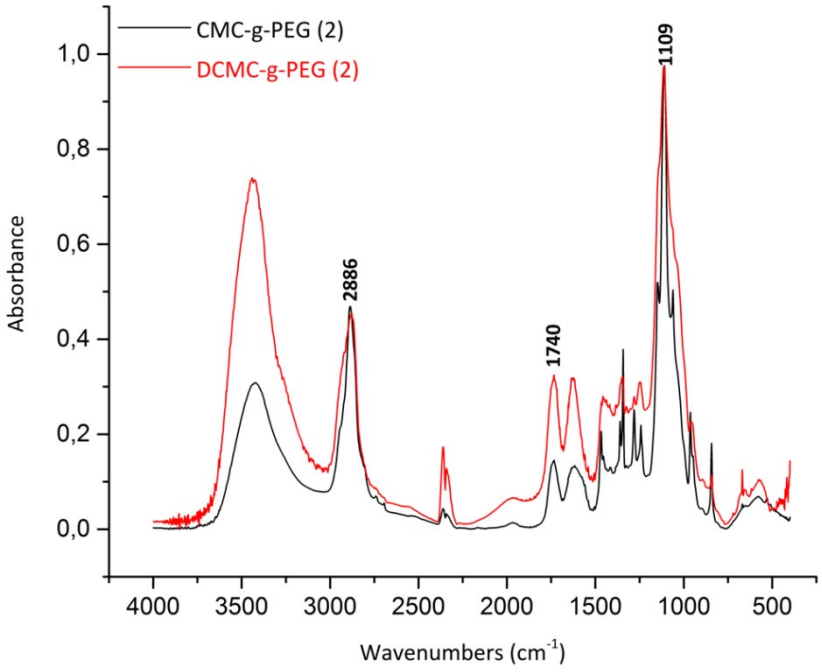

Figure A2. FTIR spectra of CMC-g-PEG (2) and DCMC-g-PEG (2).

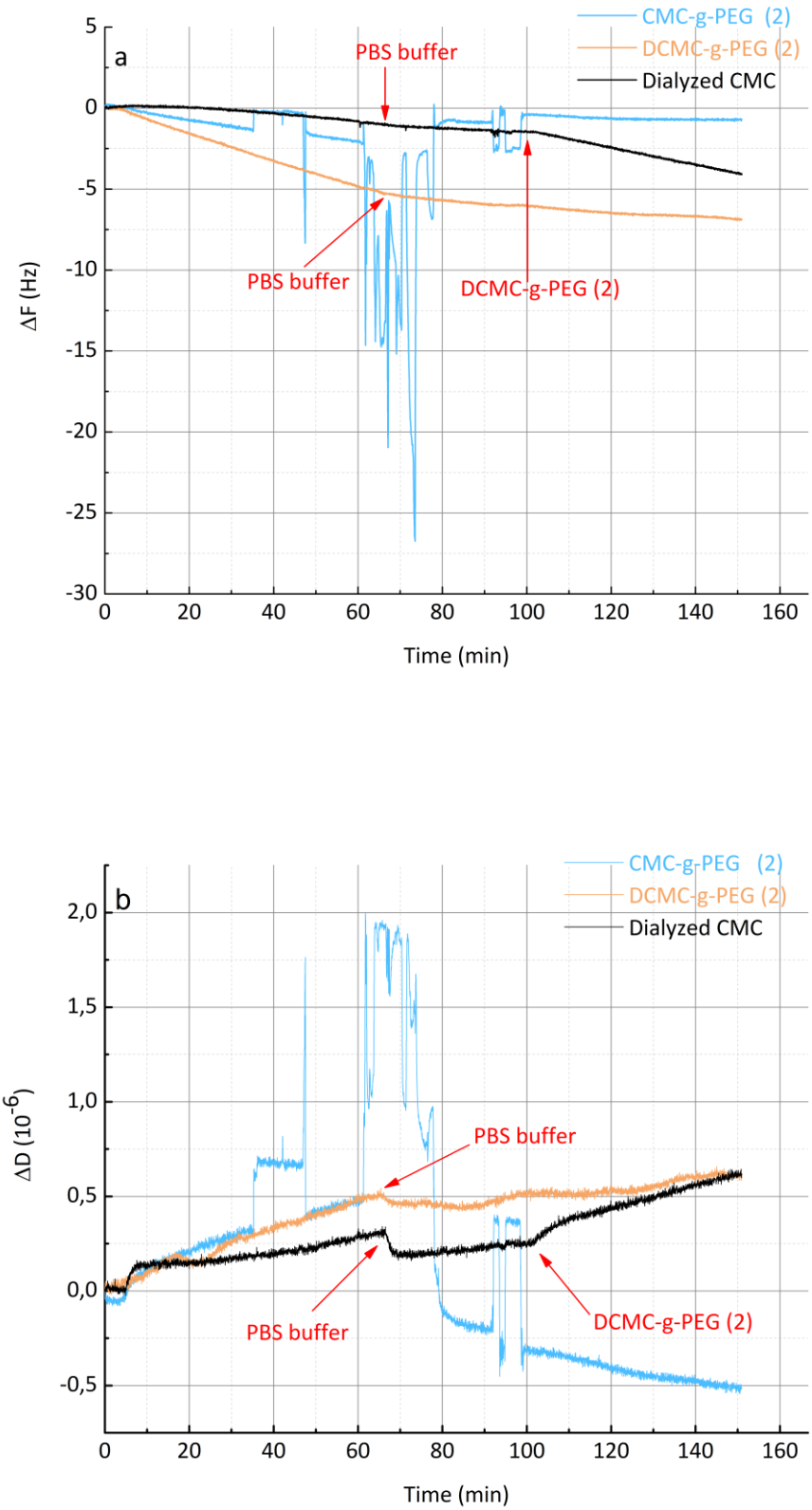

Figure A3. Frequency curves **(a)** and dissipation curves **(b)** for the adsorption of dialyzed CMC, CMC-g-PEG (2) and DCMC-g-PEG (2) onto collagen IV films. The polymer concentration was 100 μg/ml.